# Is it Time to Switch Your T1W Sequence? Assessing the Impact of Prospective Motion Correction on the Reliability and Quality of Structural Imaging

Lei Ai[1], R. Cameron Craddock[2], Nim Tottenham[3], Jonathan P Dyke[4], Stanley Colcombe[5], Michael Milham[1,5], Alexandre R. Franco[1,5,6*]

[1]Center for the Developing Brain, Child Mind Institute, New York, New York
[2]Department of Diagnostic Medicine, Dell Medical School, Austin, Texas
[3]Department of Psychology, Columbia University, New York, New York
[4]Citigroup Biomedical Imaging Center, Weill Cornell Medicine, New York, New York
[5]Center for Biomedical Imaging and Neuromodulation, Nathan S. Kline Institute for Psychiatric Research, Orangeburg, New York
[5]Department of Psychiatry, New York University School of Medicine, New York, New York

* Corresponding author: alexandre.franco@nki.rfmh.org or alexandre.franco@childmind.org

## Highlights

- The MPRAGE sequences with and without Prospective Motion Correction (PMC) are compared in a large sample size (N=419) in a "real world" scenario, where we did not explicitly ask subjects to move or maintain still during the acquisition of the structural images
- MPRAGE sequence with PMC (MPRAGE+PCM) presents higher intra-sequence reliability results in morphometric measurements compared to the traditional MPRAGE sequence without PMC.
- High inter-sequence (MPRAGE with and without PMC) reliability scores were also observed.
- Researchers are recommended use the MPRAGE+PMC as their structural T1 weighted pulse imaging sequence for future and current studies, especially in studies with hyperkinetic populations
- Due to potential higher quality control measures of the traditional MPRAGE sequence, neuroimaging researchers with low head motion participants can still consider using the MPRAGE sequence without PMC

**Abstract**

New large neuroimaging studies, such as the Adolescent Brain Cognitive Development study (ABCD) and Human Connectome Project (HCP) Development studies are adopting a new T1-weighted imaging sequence with prospective motion correction (PMC) in favor of the more traditional 3-Dimensional Magnetization-Prepared Rapid Gradient-Echo Imaging (MPRAGE) sequence. In this study, we used a developmental dataset (ages 5-21, N=348) from the Healthy Brain Network Initiative and directly compared the MPRAGE and MPRAGE with PMC (MPRAGE+PMC) sequences to determine if the morphometric measurements obtained from both protocols are equivalent or if there is an advantage to use one. The sequences were also compared through quality control measurements. Inter- and intra-sequence reliability were assessed with another set of participants (N=71) that performed two MPRAGE and two MPRAGE+PMC sequences within the same imaging session, with one MPRAGE (MPRAGE1) and MPRAGE+PMC (MPRAGE+PMC1) pair at the beginning of the session and another pair (MPRAGE2 and MPRAGE+PMC2) at the end of the session. With morphometric measurements such as volume and cortical thickness, Intraclass correlation coefficients (ICC) scores showed that intra-sequence reliability is the highest with the MPRAGE+PMC sequences and lowest with the MPRAGE sequences. Regarding inter-sequence reliability, ICC scores were higher for the MPRAGE1-MPRAGE+PMC1 pair at the beginning of the session than the MPRAGE1-MPRAGE2 pair, possibly due to the higher motion artifacts in the MPRAGE2 run. Results also indicate that the MPRAGE+PMC sequence is robust, but not foolproof, to high head motion. For quality control metrics, the traditional MPRAGE presented better results than MPRAGE+PMC in 5 of the 7 measurements. In conclusion, morphometric measurements evaluated here showed high inter-sequence reliability between the MPRAGE and MPRAGE+PMC sequences, especially in images with low head motion. Researchers conducting studies with highly kinetic populations are highly recommended to use the MPRAGE+PMC sequence, due to its robustness to head motion and higher reliability scores. However, due to potential higher quality control measures, neuroimaging researchers with low head motion participants can still consider using the MPRAGE sequence, however, can also choose to use the MPRAGE+PMC sequence to increase the reliability of the data.

## Introduction

New technologies are constantly being developed to improve the quality of Magnetic Resonance Imaging (MRI) sequences. While generally welcomed, such advances can present a significant challenge to longitudinal studies, as well as large-scale data acquisitions, both of which tend to be wary of changing methods mid-study due to the potential introduction of confounds. In light of this, choosing the optimal MRI pulse sequences for a study is always a challenging task for a neuroimaging researcher. Since its development in the early 1990s, the T1 weighted 3-Dimensional Magnetization-Prepared Rapid Gradient-Echo Imaging (3D MPRAGE, MPRAGE, or MPR) (Mugler and Brookeman 1990; Brant-Zawadzki, Gillan, and Nitz 1992) has become one of the most widely used sequence by neuroimaging researchers. This sequence, or similar sequences from other manufacturers[1], has been widely adopted for studies with large or small sample sizes. However, as all MRI imaging sequences, it is susceptible to head motion which can significantly alter the quality of the morphometry measurements that are extracted (Reuter et al. 2015; Pardoe, Kucharsky Hiess, and Kuzniecky 2016; Alexander-Bloch et al. 2016). In recent years, the MPRAGE sequence has been expanded to include volumetric navigators (vNav) in order to perform prospective motion correction (PMC) during the acquisition (Tisdall et al. 2012, 2016). The growing availability and usage of prospective PMC for structural scans (Tisdall et al. 2012). These structural sequences with navigator-based PMC have the potential to be transformative for studies involving hyperkinetic populations, such as children, the elderly, or patients with movement disorders. In particular, new large multisite studies are adopting these structural scans with PMC (see Table 1). However, the impact of the change from the traditional MPRAGE sequence to the now MPRAGE sequence with PMC has not been fully quantified (Harms et al. 2018), in part, because few datasets contain a large enough sample size with and without PMC images in the same subjects.

The ultrafast gradient-echo 3D MPRAGE pulse sequence is used by a large fraction of neuroimaging researchers because of its excellent contrast properties and capacity to collect reliable structural images (Wonderlick et al. 2009). MPRAGE can be considered as a defacto standard imaging sequence for brain morphometry studies[2]. As such, large neuroimaging studies such as the WU-Minn Human Connectome Project (HCP) (Van Essen et al. 2013)more recently referred to as the HCP Young-Adult (HCP-YA)), the NKI-Rockland Sample (Nooner et al. 2012), the UK BioBank (Sudlow et al. 2015), and the Alzheimer's Disease Neuroimaging Initiative (ADNI) (Jack et al. 2008), all use the MPRAGE sequence to collect structural T1 weighted images of the brain. While some slight differences in sequence parameters exist across studies, such as voxel size and TR/TI values, differences in parameters tend to be very similar overall (see Table 1).

For navigator-based prospective motion correction (PMC) approaches, the sequence periodically collects fast-acquisition lower resolution images (navigators) to estimate the amount and direction of head motion since the last navigator was collected. Based on the motion estimation, sequence parameters are adjusted at each repetition time (TR) to nullify this motion. For MPRAGE sequences, navigators can be collected and motion can be estimated during the

[1] MPRAGE is sequence used by Siemens MRIs and the equivalent of this sequence for GE machines is the 3-D Fast SPGR and for Philips is its 3D TFE

[2] MPRAGE is the recommended sequence to be used by Freesurfer

long inversion recovery time (TI) and applied to update the readout orientation for the current line of k-space. An early example of this method is the PROMO sequences that employs spiral acquisitions to collect navigators along the three cardinal planes of the volume (coronal, axial, and sagittal) (N. White et al. 2010). This has been extended by Tisdall et al. to use echo volume imaging (EPI applied to all 3 dimensions) to collect 3D vNav, which provide more precise motion tracking (Tisdall et al. 2012, 2016). In addition to prospectively correcting for motion that occurs between acquisitions, this sequence with PMC can also identify large motion that occurs during an acquisition. The TRs that have motion above a predefined threshold are reacquired at the end of the sequence. The maximum number of TRs that can be reacquired is set by the operator. The MPRAGE sequence with PMC (MPRAGE+PMC) has been widely adopted by research groups and more specifically, by new large imaging studies (see Table 1).

Among those most attracted to the promises of sequences with PMC are pediatric imaging researchers (S. Y. Bookheimer 2000) In particular, head motion has been shown to significantly reduce gray matter volume and thickness estimates (Reuter et al. 2015) and also alter gray matter probability scores (Gilmore, Buser, and Hanson 2019). Due to this concern, the longitudinal Adolescent Brain Cognitive Development (ABCD) Study (Casey et al. 2018) adopted the MPRAGE+PMC sequence as its standard T1-weighted structural sequence. The Healthy Brain Network (HBN) study (Alexander et al. 2017) also adopted the new MPRAGE+PMC sequence, while also maintaining the HCP style MPRAGE sequence due to concerns regarding reproducibility across sequences. The original HCP study (HCP-YA) is a project that has already concluded its data acquisition, but the study is now being expanded through the HCP Lifespan Studies. The Lifespan Studies have all converted to also collect structural imaging with the MPRAGE+PMC protocol. This includes the HCP Aging (HCP-A) (Susan Y. Bookheimer et al. 2019) for ages 36-100+ years old, the HCP Development (HCP-D) (Somerville et al. 2018) for ages 5-21 years old, and the Lifespan Baby Connectome Project (BCP) for children aged 0-5 years old (Howell et al. 2019). See Table 1 for details regarding T1-weighted structural sequences used in large neuroimaging studies.

| Study | Pulse sequence | Voxel size (mm) | Matrix Size | Num Slices | TI (ms) | TR (ms) | Bandwidth (Hz/Pz) | Parallel Imaging | Partial Fourier | Flip Angle (degrees) | Scanner |
|---|---|---|---|---|---|---|---|---|---|---|---|
| Rockland Sample | MPRAGE | 1.0x1.0x1.0 | 256x256 | 176 | 900 | 1900 | 170 | 2 | off | 9 | Tim-Trio |
| UK Biobank | MPRAGE | 1.0x1.0x1.0 | 256x256 | 208 | 880 | 2000 | 240 | 2 | off | 8 | Siemens 3T Skyra |
| ADNI3 | MPRAGE | 1.0x1.0x1.0 | 256x240 | 176 | 900 | 2300 | 240 | 2 | off | 9 | Many |
| WU-Minn HCP [a.k.a HCP-YA] | MPRAGE | 0.7x0.7x0.7 | 320x320 | 256 | 1000 | 2400 | 210 | 2 | off | 8 | Custom HCP Skyra |
| HCP Aging (HCP-A) And Development (HCP-D) | MPRAGE | 0.8x0.8x0.8 | 320x300 | 208 | 1000 | 2500 | 220 | 2 | off | 8 | Prisma |
| | MPRAGE +PMC | 0.8x0.8x0.8 | 320x300 | 208 | 1000 | 2500 | 740 | 2 | 6/8 (slice partial fourier) off for phase | 8 | Prisma |
| HCP Baby (BCP)* | MPRAGE | 0.8x0.8x0.8 | 320x320 | 208 | 1060 | 2400 | - | - | - | 8 | Prisma |

| | | | | | | | | | | | |
|---|---|---|---|---|---|---|---|---|---|---|---|
| ABCD | MPRAGE +PMC | 1.0x1.0x1.0 | 256x256 | 176 | 1060 | 2500 | 240 | 2 | off | 8 | Prisma |
| Healthy Brain Network (HBN) ** | MPRAGE | 0.8x0.8x0.8 | 320x320 | 224 | 1060 | 2500 | 130 | 2 | 7/8 (slice partial fourier) off for phase | 8 | Prisma |
| | MPRAGE +PMC | 1.0x1.0x1.0 | 256x256 | 176 | 1060 | 2500 | 240 | 2 | off | 8 | Prisma |

Table 1. T1-weighted structural imaging parameters across large imaging studies. Only reporting imaging sequences performed on 3T Siemens MRIs.
* We were unable to find all the sequence parameters for the BCP. However, the researchers of BCP state they attempt to match as much as possible the imaging parameters of the other HCP studies (Howell et al. 2019).
** For the HBN study, currently only one of the imaging sites (Citigroup Biomedical Imaging Center - CBIC) is collecting two structural scans for all subjects.

Given that new large imaging studies (i.e. HCP Lifespan and ABCD) are using the MPRAGE+PMC sequence to collect their structural data, we raise a key question, should other researchers switch from the well-established MPRAGE sequence to the MPRAGE+PMC sequence? In this study, we present quantifiable similarities and differences between the HCP style MPRAGE to the ABCD style MPRAGE+PMC sequence to address the previous question.

## Methods

### Neuroimaging Data

All neuroimaging data used in this study were collected as part of the Healthy Brain Network (HBM) Project (Alexander et al. 2017) and were acquired on a Siemens Prisma Fit with a 32 channel head coil located at the Citigroup Biomedical Imaging Center (CBIC) at Weill Cornell Medicine. A total of 465 imaging sessions were analyzed. Of these 465 participants, 348 completed the full HBN MRI protocol and are included in this study, with an age range of 5 to 21 years old (mean=11.3±3.6) which included 120 females and 228 males. The HBN protocol at CBIC includes two structural T1-weighted sequences, one based on the Human Connectome Project-YA (here referred to as the “MPRAGE” sequence), and another based on the ABCD study with the MPRAGE sequence with PMC (here referred to as the “MPRAGE+PMC” sequence).

Another set of participants (N=71) performed a test-retest protocol (Test-Retest Group). As part of the protocol specifically designed for this study, these participants performed two MPRAGE scans and two MPRAGE+PMC scans within the same imaging session. Specifically, one MPRAGE+PMC (MPRAGE+PMC1) and then one MPRAGE (MPRAGE1) sequence were performed at the beginning of the imaging session and the other two sequences were repeated at the end of the imaging session (MPRAGE2 and then MPRAGE+PMC2). This strategy was chosen since a larger amount of head motion is expected on the runs at the end of a session. The test-retest group had an age range of 5 to 20 years old (mean=11.6±3.7) with 23 females and 42 males. The HBN protocol and timing of the sequences for both groups are provided in Supplementary Tables 1 (ST1) and 2 (ST2).

Imaging Parameters

The MR Protocol Guidance from the Human Connectome Project (Glasser et al. 2016) was followed to define the 3D MPRAGE HCP style imaging sequence. For the structural sequences with the navigators (MPRAGE+PMC), we used the protocol from the ABCD study (Casey et al. 2018). The imaging sequence protocol parameters used in this study are shown in Table 1. Additionally, for the MPRAGE+PMC sequence, we configured the sequence with a reacquisition threshold of 0.5 (see equation [3] in (Tisdall et al. 2012)) and up to 24 TRs could be remeasured. The MPRAGE sequence had a duration of 7 minutes and 19 seconds, while the MPRAGE+PMC can take up to 7 minutes and 12 seconds to be acquired. During the structural runs, the participants were shown the Inscapes Movie (Vanderwal et al. 2015), a video developed to improve compliance related to motion and wakefulness.

Structural Quantitative Measurements

We extracted morphometry measurements from the images using Mindboggle (Klein et al. 2017). Within Mindboggle, Freesurfer (Fischl 2012) measures were also extracted. For each Freesurfer label, measurements included volume, area, median travel and geodesic depth, and the median measurement of Freesurfer's cortical thickness, curvature, and convexity of the sulcus (Fischl 2012). Geodesic depth is the shortest distance along the surface of the brain from the point to where the brain surface makes contact with the outer reference surface (Klein et al. 2017), whereas travel depth is the shortest distance from a point to the outer reference surface without penetrating any surface (Giard et al. 2011; Klein et al. 2017). Total gray matter volume across different structural runs was also measured with FSL's SIENAX (Smith et al. 2002) package, in addition to the results obtained through Mindboggle.

Reliability

Intraclass correlation coefficients (ICC(3,1)) was used to calculate the reliability of the morphometric measures (Shrout and Fleiss 1979). Inter-sequence reliability was measured between the different imaging sequences, MPRAGE and MPRAGE+PMC. Intra-sequence reliability was measured across different imaging runs for the same pulse sequence.

Age-Related Changes

We estimated age-related changes to compare the two imaging sequences. Age-related curves were separated by sex and by the quantity of motion during the functional sequences.

Quality Control

Six measures of quality control for the structural images were performed by using the Quality Assessment Protocol (QAP) toolbox (Zarrar et al. 2015). Specificall, for each subject and structural image the following quality control scores measures were calculated:

- Contrast to Noise Ratio (CNR): measures the mean of the gray matter intensity values minus the mean of the white matter intensity values divided by the standard deviation of the values outside the brain) (Magnotta, Friedman, and FIRST BIRN 2006);
- Signal to Noise Ratio (SNR): measures the mean intensity within the gray matter divided by the standard deviation of the values outside the brain)(Magnotta, Friedman, and FIRST BIRN 2006);

- Foreground to Background Energy Ratio (FBER): measures the variance of voxels inside the brain divided by the variance of voxels outside the brain;
- Percent Artifact Voxels (PAV): measures the proportion of voxels outside the brain with artifacts to the total number of voxels outside the brain (Mortamet et al. 2009);
- Smoothness of Voxels (FWHM) measures the full-width half maximum of the spatial distribution of the image intensity values in voxel units (Magnotta, Friedman, and FIRST BIRN 2006);
- Entropy Focus Criterion (EFC), measures the Shannon entropy of voxel intensities proportional to the maximum possible entropy for a similarly sized image; Indicates ghosting and head motion-induced blurring) (Atkinson et al. 1997).

For the CNR, SNR, and FBER, a higher score means a better image, while for the FWHM, PAV, and EFC, a lower score is better.

An additional quality control measurement was also performed that is not part of the QAP package. Specifically, we compared the background noise in two regions around the brain. One 12mm radius circle located in front of the forehead immediately above the eyeball (Anterior ROI), and another above the head (Superior ROI) (See Supplementary Figure SF1 for the location of the circles). We then calculated the ratio of the average signal from the Anterior divided the Superior region of interest, hence Anterior-to-Superior Ratio (ASR). For ASR, a lower score is better.

Motion estimation

EPI volumetric navigators with an 8mm isotropic resolution are collected with the MPRAGE+PMC pulse sequence. These volumes are used as navigators to estimate the head motion during the scan, and one three dimensional volume is acquired at each TR. For the HBN study, the total number of volumes that were acquired at each MPRAGE+PMC sequence range from 143 to 168, depending on the number of TRs that need to be reacquired based on subject motion (Tisdall et al. 2012). For each MPRAGE+PMC run, the framewise displacement (FD) (Jenkinson et al. 2002) was calculated with these EPI volumes. The FD was then converted to FD per minute ($FD_{pm}$) by (Tisdall et al. 2012):

$$FD_{pm} = \frac{\sum_{i=2}^{N} FD(i-1,i)}{N \cdot TR} \cdot 60$$

where *N* is the number of TRs, *TR* is the repetition time in seconds, *i* is the volume, and *FD(i-1,i)* is the FD between two subsequent volumes.

With the MPRAGE sequence, we cannot directly estimate motion, hence we investigated if the average motion across all functional scans can be used as a proxy for how much a participant moves during a structural scan. Specifically, the average $FD_{pm}$ for all functional MRI scans of the protocol were also calculated and compared.

## Results

How do the sequences compare by visual inspection?

By visual inspection, there were some key differences in image intensity and quality when comparing the MPRAGE and MPRAGE+PMC sequences (Figure 1). For the purposes of demonstration, through visual inspection of the structural images, we identified two participants,

one with a low amount of motion (Non-Mover) and one with a high amount of motion (Mover). For the participant data on the left (Non-Mover), visually, the images appear to be of excellent quality for both the MPRAGE and MPRAGE+PMC sequences. This subject had a low amount of motion during the data collection of the MPRAGE+PMC sequence ($FD_{pm}$ = 6.04 during MPRAGE+PMC sequence). For the functional scans of the protocol, the same participant has a low $FD_{pm}$ = 7.24 (see *Motion Estimation* section below on how head motion was estimated for the MPRAGE runs). The images on the right represent a participant with a large amount of motion for the MPRAGE and MPRAGE+PMC sequence. Even though there was a large amount of head motion during the acquisition in the MPRAGE+PMC sequence ($FD_{pm}$ = 62.23 during MPRAGE+PMC sequence; average $FD_{pm}$=17.41 during functional scans), the quality of the T1's is still sufficient for many applications. That is not the case for the MPRAGE images, where the ringing artifacts are strikingly pronounced and this data would have to be discarded for any neuroimaging study. However. it is important to note that for the MPRAGE+PMC image, the gray-white matter boundaries are not as sharp as the low motion subject. There are also some ringing artifacts present in the MPRAGE+PMC image. Hence, the MPRAGE+PMC image is not completely immune to head motion, as seen in Figure 1 and also in Supplementary Figure SF2.

---

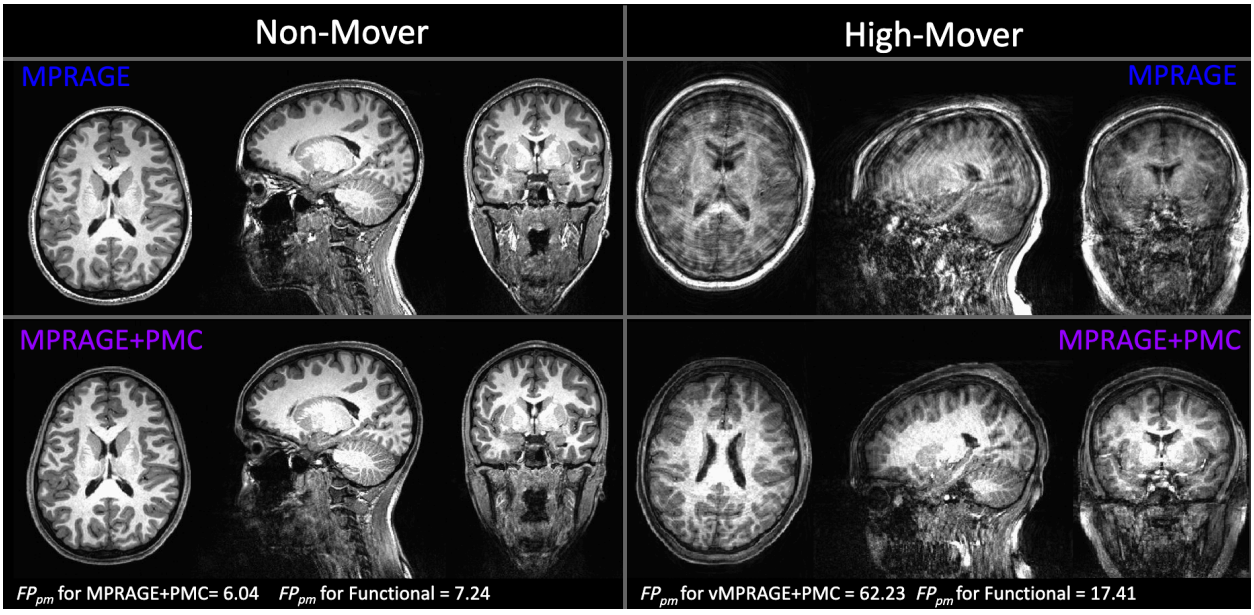


Figure 1. T1 structural images for the two sequences, MPRAGE and MPRAGE+PMC. The top row shows the MPRAGE sequence, while the bottom row shows the images that were generated with the MPRAGE+PMC sequence. Columns represent two different participants, one with minimal head motion (left, Non-Mover) and another with a large quantity of motion (right, High-Mover).

---

Does the Surface Reconstruction Complete?

A first simple, however very practical, comparison of these two sequences is to test whether Mindboggle was able to complete processing the surface reconstruction. With images of poor quality, such as the one seen for the "Mover" subject in the MPRAGE sequence (Figure 1), the software does not complete and returns an error instead of the morphometry measurements.

For the large group, a total of 346 participants completed both the MPRAGE and MPRAGE+PMC sequences. Of the 346 images, Mindboggle successfully completed surface reconstruction in 89.3% (N=309) of the MPRAGE images and 91.6% (N=317) of the MPRAGE+PMC images. Using McNemar's test (McNEMAR 1947), no statistically significant differences ($p>0.1$) were found between completing the processing of the images for the different sequences. We visually inspected the 31 images from the MPRAGE+PMC images that did not complete surface reconstruction and all looked blurry (see examples in Supplementary Figure SF2). The average motion from the EPI navigators of the MPRAGE+PMC sequences was then calculated. For the images that completed the surface reconstruction, there was an $FD_{pm}$ = 13.70 +- 12.85, while for the images that were not completed the motion was much higher, with an $FD_{pm}$ = 47.56 +- 37.32. For the subsequent analysis shown in this manuscript that depend on the surface reconstruction results, only the data from participants that Mindboggle was able to complete processing both images are used. Therefore, 290 subjects (105 females, mean age = 11.20 +- 3.66, age range = [5.44, 20.47]) are included in the following analyses that depend on surface reconstruction estimates. Hence, the following results that are presented only use data that has already passed through a first level of quality control, i.e. completing surface reconstruction.

For the test-retest group, we performed the same type of quality control analysis, but now with sequences that were collected closely within the session, with the MPRAGE1 and MPRAGE+PMC1 at the beginning of the session and MPRAGE2 and MPRAGE+PMC2 at the end. Of the 72 participants that completed all four runs, Mindboggle completed processing on 94.5% (N=68) of the MPRAGE1, 98.6% (M=71) of the MPRAGE+PMC1, 97.2.6% (N=70) of the MPRAGE2, and 97.2% (N=70) of the MPRAGE+PMC2. Again, using McNemar's test we found no statistically significant differences ($p>0.1$) between the sequences regarding Mindboggle completing the processing of the images. Mindboggle was able to calculate morphometric measurements in all 4 structural runs for 65 participants. These participants are used in the reliability tests shown below.

Reliability

Intra- and inter-sequence reliability results for the Mindboggle measurements are shown in Figure 2. ICC scores are shown for each of 62 cortical regions defined by Freesurfer (list of regions can be seen in supplementary table ST3) and for the following measurements, (1) area, (2) Freesurfer median cortical thickness, (3) travel depth, (4) geodesic distance, (5) curvature, and (6) convexity. The first row shows results for all participants. They were then divided into two groups, through a median split of the mean $FD_{pm}$ of the functional scans. The Intra-sequence reliability of cortical measures extracted from the MPRAGE+PMC sequences was better for all of the regions and measures compared to the MPRAGE pair. This is possibly due to a higher motion during the MPRAGE2 scan, which was collected at the end of the session. Another noticeable result is that even for the low motion subjects, the ICC was higher for the MPRAGE1 x

MPRAGE+PMC1 pair (inter-sequence) compared to the MPRAGE1 x MPRAGE2 pair (intra-sequence). Again, this is possibly due to the higher motion in the MPRAGE2 runs, even though these were the subjects with lower motion estimation scores. Also, from the same reproducibility results it is important to notice that even though the voxel sizes are of different sizes for the MPRAGE ($0.512mm^3$) and MPRAGE+PMC ($1mm^3$) sequences, the ICC scores between MPRAGE1 and MPRAGE+PMC1 are higher than repeating the MPRAGE sequence.

---

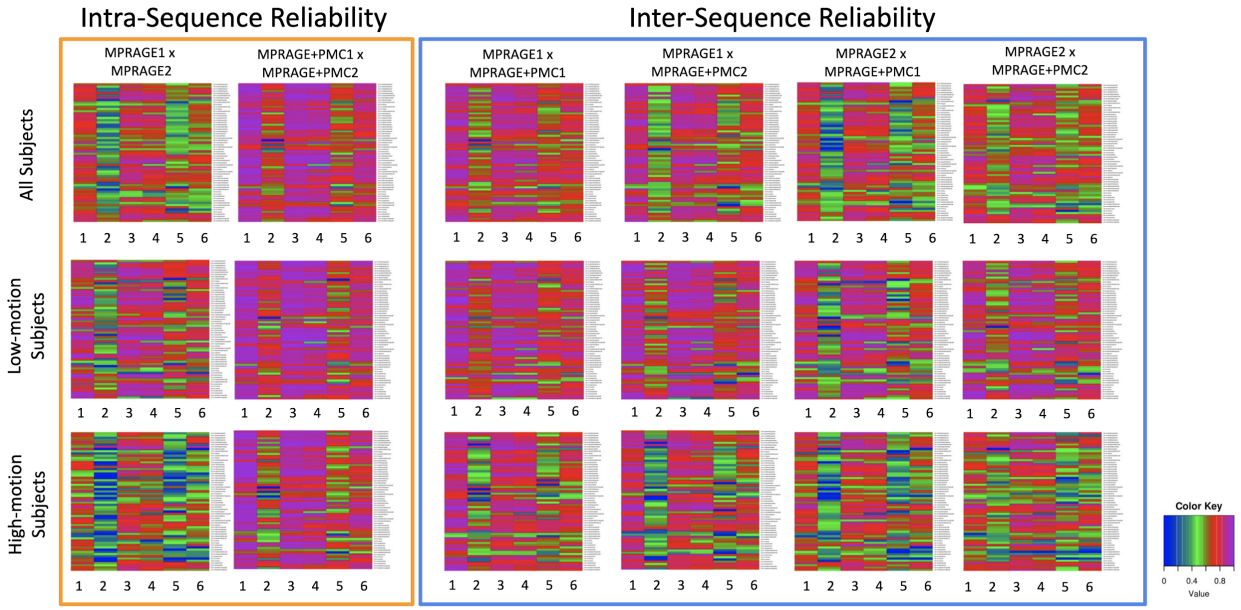


Figure 2. Test-retest reliability and reproducibility ICC results for Mindboggle measurements within each of Freesurfer 62 cortical regions. Measurements tested were (1) area, (2) Freesurfer median cortical thickness, (3) travel depth, (4) geodesic distance, (5) curvature, and (6) convexity.

---

Histogram plots of ICC for the area, volume, and Freesurfer median cortical thickness across all brain regions are shown in Figure 3. As can be seen in the histograms, the pair MPRAGE+PMC1 x MPRAGE+PMC2 (orange line) outperformed the ICC scores of all other pairs. It is clear that the reproducibility between MPRAGE+PMC1 and MPRAGE+PMC2 is high, with an average ICC score above 0.8 for Area and Volume and above 0.6 for cortical thickness. The pair MPRAGE1 x MPRAGE+PMC1 (green line) typically showed the second-best performance. The lower ICC scores in the low-motion and high-motion subjects for any pair that contains the MPRAGE2 run (blue, purple, and brown lines) is highly observable, especially for Area. The MPRAGE+PMC2 run is also performed at the end of the session, however contrary to MPRAGE sequence, and we can directly measure the amount of motion during that run. During the MPRAGE+PMC2 run, on average, there is at least twice the amount of head motion ($FD_{pm}$ = 7.5 for MPRAGE+PMC1 and $FD_{pm}$ = 15.34 for MPRAGE+PMC2). Also, when considering the pairs that contain the MPRAGE2 run, there is a large negative shift in ICC scores when comparing the "Low-Motion" and "High-Motion" subjects. With the other pairs, there is also a negative shift in

ICC scores, but at a much smaller scale. These results corroborate with the notion that the MPRAGE+PMC is more robust to motion compared to the sequence without PMC.

ICC of Cortical Thickness was worse for all pairs compared to Area and Volume. This shows how sensitive the measurement of Cortical Thickness is, especially in regard to head motion. The improvement in ICC for the MPRAGE+PMC pair over the MPRAGE pair was unanticipated for the low motion group, given that the MPRAGE sequence has a better spatial resolution, which is expected to obtain better cortical thickness estimation results. Another key result from the "ideal" low motion group, is that the inter-sequence pairs MPRAGE1-MPRAGE+PMC1 (green line) and MPRAGE1-MPRAGE+PMC2 (red line) show higher reliability than the intra-sequence pair MPRAGE1-2 (blue line) for all the three measures being evaluated.

---

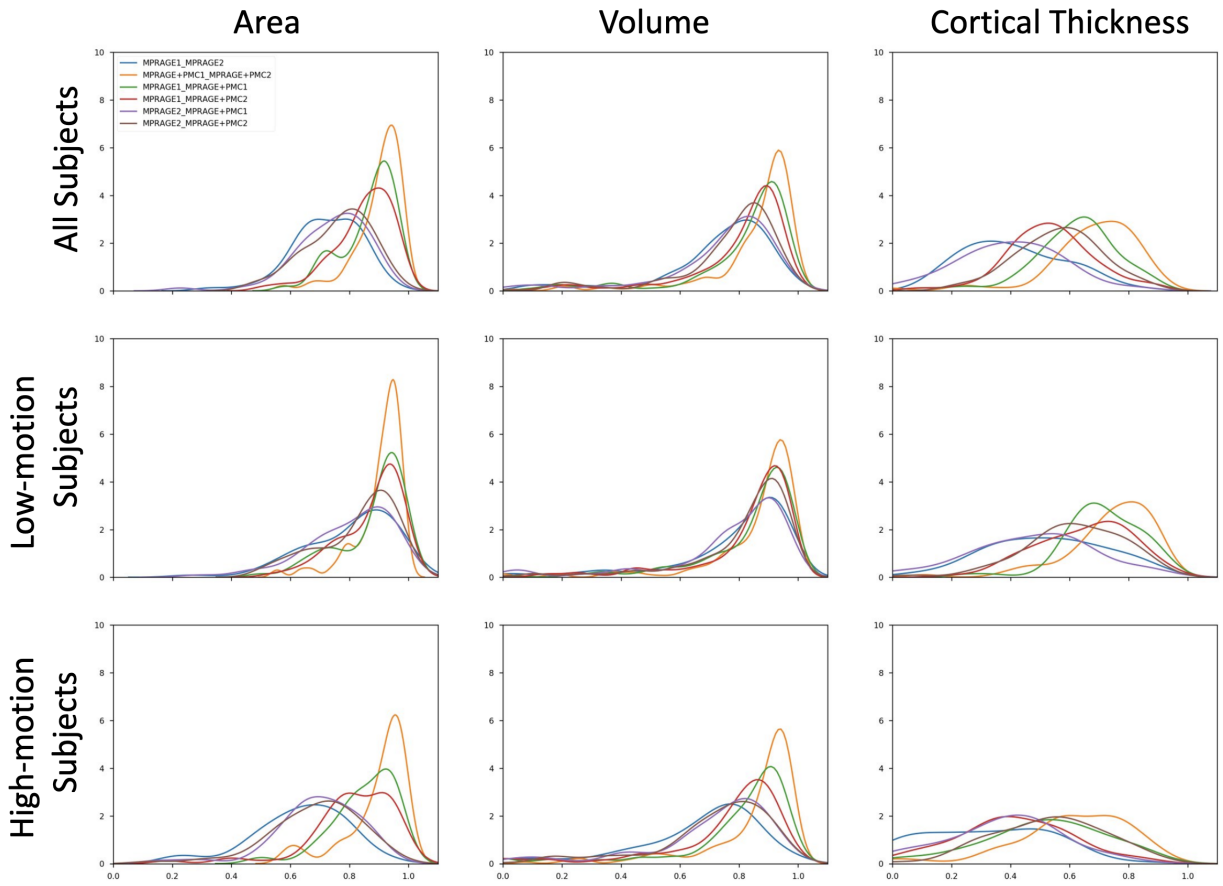


Figure 3. Histogram plots of ICC for the test-retest group that performed two MPRAGE scans and two MPRAGE+PMC scans within the same session. ICC is calculated for Area, Volume and Cortical Thickness.

---

The impact of acquisition sequence on gray matter volume estimation was evaluated using Freesurfer and SIENAX (Figure 4) with the test-retest dataset. Pairwise comparisons were made

for each combination by calculating the absolute difference in volume measures. MPRAGE+PMC1 and MPRAGE+PMC2 had the most similar gray matter volumes for both toolboxes. The largest differences were observed in the pairs that included the MPRAGE2 image. These results indicate that the prospective motion correction sequence is robust for measuring gray matter volume regardless of the toolbox used to calculate volumes. It also endorses the assumption that the MPRAGE+PMC sequence provides us more reliable results compared to MPRAGE, independent on when the structural sequence is performed within the session, beginning or end.

---

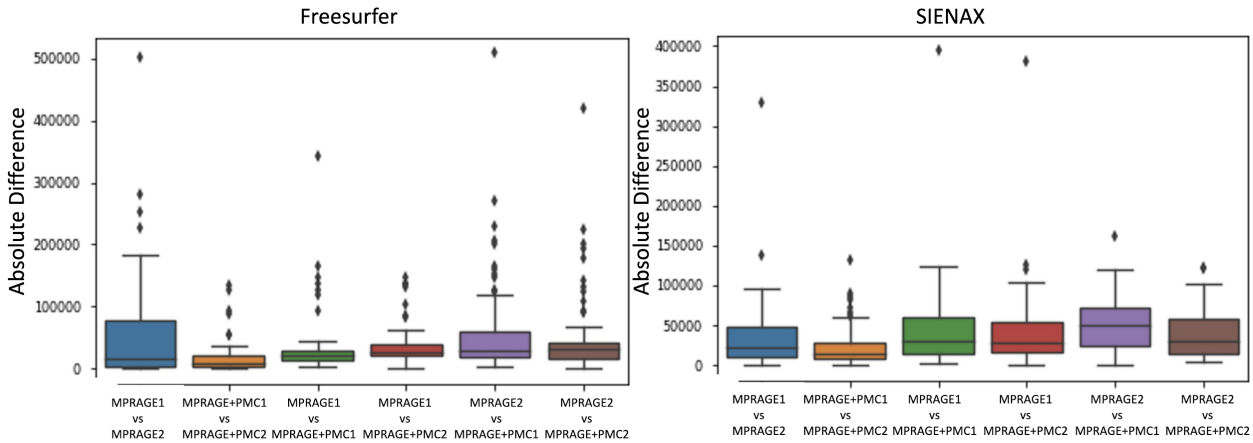


Figure 4. The absolute difference in gray matter volume within the test-retest group. Gray matter was measured using MindBoggle and SIENAX.

---

How does Motion Affect Structural Measurements Between Sequences?

With the larger dataset, we performed an analysis to investigate if the differences in measurements of cortical thickness are affected by head motion. For each region, a correlation was calculated between the difference in cortical thickness measured with the MPRAGE and MPRAGE+PMC images (MPRAGE - MPRAGE+PMC) and the mean $FD_{pm}$ across the functional scans. For males, 26 regions showed a statistically significant correlation ($p<0.05$) of the difference in cortical thickness measurements and head motion. The grand majority of these regions, especially in the frontal lobe, showed a negative correlation (n=24). There were two areas in the occipital lobe that show a positive correlation. These results indicate that, as there was an increase in subject head motion, the difference in the measurement of cortical thickness between MPRAGE and MPRAGE+PMC increases, with a larger cortical thickness estimate with the MPRAGE+PMC sequence in 24 areas (see Figure 5, Supplementary Table ST3 for list of regions, and scatter plots are shown in Supplementary Figures SF3 and SF4). For females, 31 regions showed a significant negative correlation between the difference in cortical thickness and motion estimation. No areas showed a positive correlation for females.

---

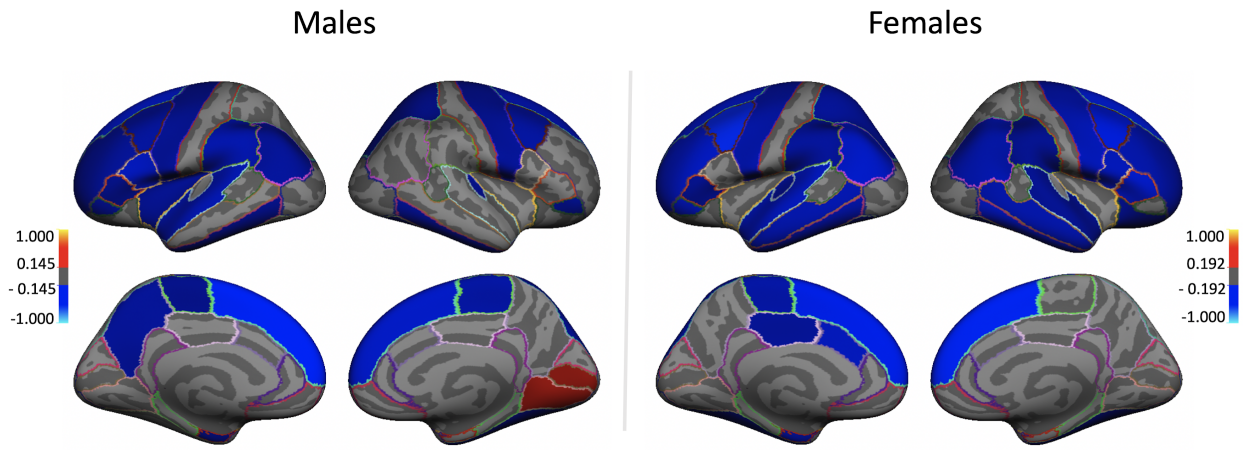


Figure 5 - Freesurfer regions that showed a significant correlation ($p<0.05$) between the difference in cortical thickness measurements (MPRAGE-MPRAGE+PMC) and mean FD across the functional scans.

---

We also calculated pairwise t-tests to compare the cortical thickness measurements between MPRAGE and MPRAGE+PMC in the 62 cortical regions defined by Freesurfer. For males, there was a significant difference ($p<0.05$) in 38 of the 62 regions. Of the 38, 27 showed a larger cortical thickness for MPRAGE and 11 for MPRAGE+PMC (Supplementary Figure SF5). For females, 38 regions also presented differences in cortical thickness measurements, with 29 showing greater cortical thickness for MPRAGE and 9 for MPRAGE+PMC (Supplementary Figure SF5). Statistical scores for all the regions are shown in Supplementary Table ST4.

Age-Related Differences

Figure 6 shows development curves for total volume, gray and white matter volume, and ventricle volume for male and female participants. Only a smaller subset of subjects (N=248, 92 females) was used to calculate the development curves since there were very few subjects older than 16 to obtain adequate development estimation curves at higher ages. Hence, development curves are shown only for ages 6 to 16. Black dots represent volumes calculated with the MPRAGE sequence while red dots represent the MPRAGE+PMC sequence. For each sequence, a quadratic curve was fit for estimating development growth. For the “All Subjects” the development graphs are similar for both imaging sequences. With a median split, participants were grouped by low and high motion. Even for the subjects with large motion, the development curves are similar, just deviating at the higher ages for both groups. This deviation in curvature is possibly due to the low number of subjects that are older with a higher amount of motion. The development curves are shown for cortical thickness measurements for males and females are shown in Supplementary Figures SF6 and SF7, respectively.

---

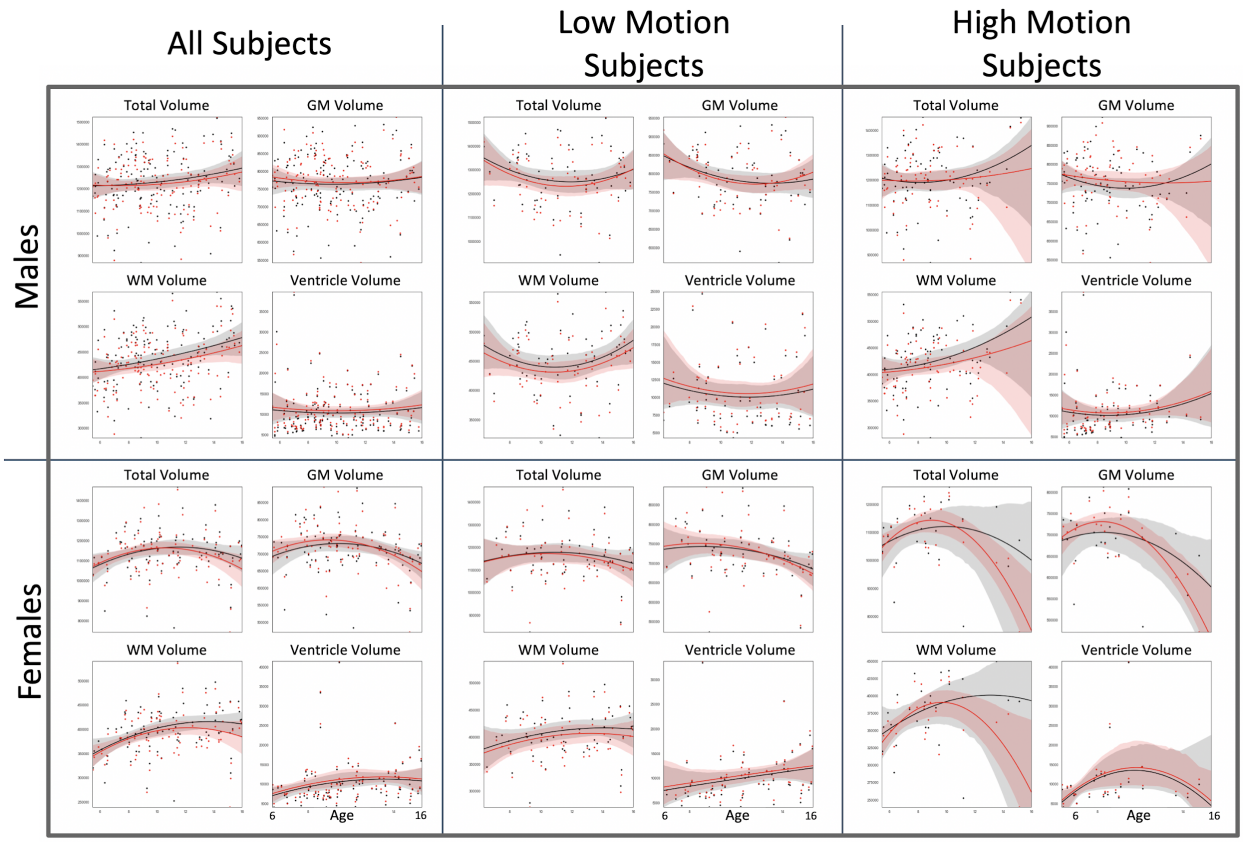


Figure 6. Black dots and lines (with 95% confidence intervals) are developmental measures for the MPRAGE sequence, while the red dots and lines are for the MPRAGE+PMC sequence.

---

Quality Control Metrics

The MPRAGE+PMC sequence is identical to the MPRAGE sequence, except for the inclusion of a navigator acquisition and registration block, lasting 355 milliseconds, during the inversion recovery time and just before the parent sequence's readout (Tisdall et al. 2012). In previous comparisons between these sequences, the MPRAGE+PMC sequence resulted in an approximately 1% reduction in contrast and a 3% reduction in image intensities (Tisdall et al. 2012). Importantly, these reductions were spatially uniform, so did not increase regional variation in image intensity (e.g., the 'bias' field). The MPRAGE+PMC sequence has been shown to result in more artifacts, such as ghosting, in the background, but since they did not overlap with the brain, they were not considered problematic (Tisdall et al. 2012).

In our study, acquisition parameters were identical between sequences, with the exception of voxel resolution, bandwidth, and partial Fourier. These differences are a consequence of MPRAGE+PMC's navigate and register block reducing the amount of time available for parent sequence readout. From MRI theory, SNR is proportional to voxel volume (V) and inversely proportional to the square root of bandwidth (BW) and the square root of the partial Fourier reduction factor (R). The relative SNR from the MPRAGE+PMC sequence to the MPRAGE sequence can be calculated by:

$$\frac{SNR_{vNav}}{SNR_{MPRAGE}} = \frac{\frac{V_{vNav}}{\sqrt{BW_{vNav}}\sqrt{R_{240}}}}{\frac{V_{MPRAGE}}{\sqrt{BW_{MPRAGE}}\sqrt{R_{MPRAGE}}}} = \frac{\frac{1^3}{\sqrt{240}\sqrt{1}}}{\frac{0.8^3}{\sqrt{130}\sqrt{1.14}}} = 1.54$$

From these relationships, the SNR of the MPRAGE+PMC sequence is expected to be about 1.54 times greater than the SNR of the MPRAGE sequence (Craddock et al. 2013; Brown et al. 2014).

Figure 7 and shows the QAP quality control metrics for the 348 participants. Quality control metrics for the test-retest group are shown in Supplementary Figure SF8. Paired t-test were calculated at each measure to statistically compare sequences. Results showed significant differences ($p<0.05$) for all measures and are shown in Table 2. When comparing MPRAGE and MPRAGE+PMC, MPRAGE+PMC had a better score for CNR and ASR. MPRAGE exhibited a better score in all the other measures.

These results are a bit unexpected, especially for SNR, since theoretically the MPRAGE+PMC sequence should have an SNR 1.54 times greater than MPRAGE. Tisdal et. al (Tisdall et al. 2012) reported that the MPRAGE+PMC images had an increased ghosting effect that was only observed in the background. We are calculating SNR of each image by measuring the mean intensity within the gray matter and dividing by the standard deviation of the voxels outside of the brain. The increase in ghosting artifacts in the background would justify the reduction in SNR for the MPRAGE+PMC images. The same holds for justifying the inferior scores for MPRAGE+PMC in FBER, PAV, and EFC, which all depend on the background signal to calculate their metrics. The larger receive bandwidth (RBW) of the MPRAGE+PMC sequence (240 kHz) compared to the RBW of the MPRAGE (130 kHz) might justify the increase in background noise, since a larger RBW lets in more noise in the echo. The lower FWHM scores for the MPRAGE image are due to smaller voxel sizes compared to the MPRAGE+PMC image.

---

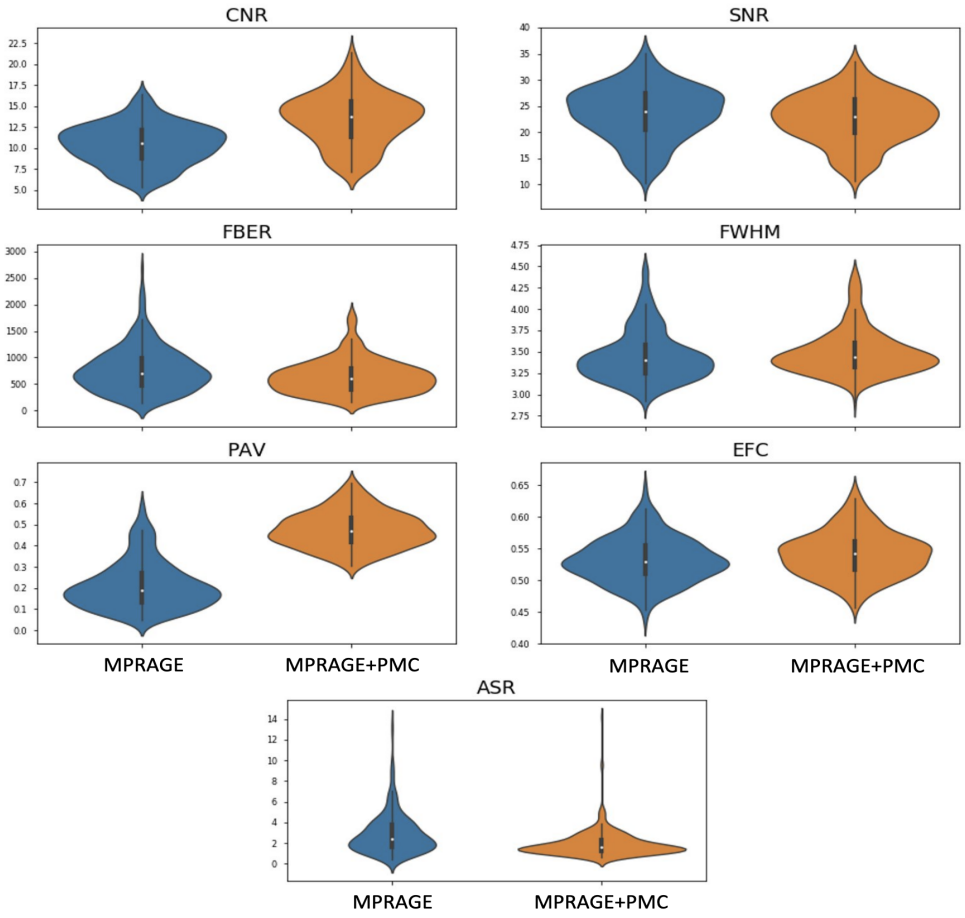


Figure 7. QAP metrics for the MPRAGE and MPRAGE+PMC images across 287 participants. Quality control metrics include; Contrast to Noise Ratio (CNR), Signal to Noise Ratio (SNR), (FBER), Smoothness of Voxels (FWHM), Percent Artifact Voxels (PAV), Entropy Focus Criterion (EFC), and Anterior-to-Superior Ratio (ASR).

---

| QAP Measure | Contrast | t-score | P-value (uncorrected) |
|---|---|---|---|
| CNR | MPRAGE-MPRAGE+PMC | -18.06 | 2.08E-47 |
| SNR | MPRAGE-MPRAGE+PMC | 3.45 | 6.46E-4 |
| FBER | MPRAGE-MPRAGE+PMC | 7.23 | 5.55E-12 |
| FWHM | MPRAGE-MPRAGE+PMC | -2.93 | 3.74E-3 |
| PAV | MPRAGE-MPRAGE+PMC | -40.08 | 1.40E-111 |
| EFC | MPRAGE-MPRAGE+PMC | -8.00 | 4.57E-14 |
| ASR | MPRAGE-MPRAGE+PMC | 7.88 | 7.06E-14 |

Table 2. Paired t-test results comparing each of the QAP metrics; Contrast to Noise Ratio (CNR), Signal to Noise Ratio (SNR), Foreground to Background Energy Ratio (FBER), Smoothness of Voxels (FWHM), Percent Artifact Voxels (PAV), Entropy Focus Criterion (EFC), and Anterior-to-Superior Ratio (ASR). The t-scores and p-values are color coded to indicate which image (MPRAGE or MPRAGE+PMC) performed better at each paired comparison.

Motion Estimation

Head motion occurring during fMRI scans has been proposed as a surrogate for sMRI motion when no other method for estimating motion from the data exists (Pardoe, Kucharsky Hiess, and Kuzniecky 2016). The potential accuracy of fMRI as a surrogate of sMRI motion is supported by observations of high test-retest reliability for motion parameters across scans and sessions (Yan et al. 2013). But, fatigue, discomfort and other factors are known to increase motion over time, which will likely degrade the surrogate's accuracy. We directly tested the validity of using fMRI motion as a surrogate for sMRI motion by correlating sMRI motion estimates from the MPRAGE+PMC sequence with motion from each of the fMRI scans collected in the same session with the test-retest dataset (see Supplementary Tables ST1 and ST2 and Alexander (Alexander et al. 2017) for details on the full imaging session.). We additionally tested how well the average motion across all fMRI scans correlates with the motion calculated in the MPRAGE+PMC run (Figure 8). In Figure 8 runs are listed in the order that there were collected.

The leftmost column of Figure 8 shows the average $FD_{pm}$. As expected, there is a tendency for an increase in head motion as the session prolonged. There were two runs that were repeated

in the first half and in the second half of the session, MPRAGE+PMC1-2 and peer1-3[3]. For the MPRAGE+PMC runs, there was an increase in average $FD_{pm}$ from 7.50 to 15.34 for MPRAGE+PMC1 and MPRAGE+PMC2 respectively. A large increase in motion also occurs for the peer runs, from 11.29 in peer1 to 17.43 in peer3. An exception to this increase in head motion was MovieTP, which is a short animated and engaging movie ("The Present"), which could have been the reason for lower head motion during that run.

Results indicate that runs which were collected close in time showed higher correlations than runs that were collected farther apart. For example, rest1 has a much higher correlation with peer1 in $FD_{pm}$ (r=0.79) which is collected immediately after rest1, than it did to movieTP (r=0.40) which occurred at the very end of the scanning session. The exception to this order effect was rest1 and movieDM, which were separated in time, with a correlation of r=0.80. The average $FD_{pm}$ across the functional runs ("Mean") exhibited a high correlation with all the runs, with values ranging from r=[0.41, 0.83]. The correlation of $FD_{pm}$ with the two structural runs was r=0.41 and r=0.7 for MPRAGE+PMC1 and MPRAGE+PMC2, respectively. Therefore, as previously suggested, the mean FD across the functional scans is a decent surrogate measure for the head motion for the structural scans (Pardoe, Kucharsky Hiess, and Kuzniecky 2016).

---

[3] Peer (Peer Eye Estimation Regression) is a short (<2 minutes) functional run to calibrate an fMRI-based eye tracking algorithm. See (Son et al. 2019) for more details. In the initial HBN protocol, there was a peer2 run which was later dropped due to time constraints and no need to have 3 calibration runs.


Figure 8. Correlation of the $FD_{pm}$ of all the runs. The main diagonal shows the distribution of $FD_{pm}$ each run (MPRAGE+PMC1 to movieTP) and the average $FD_{pm}$ of the functional runs ("Mean"). The bottom left of the diagonal shows the scatter plot of the motion parameters across runs, while the top right of the diagonal. The values on the left column shows the average $FD_{pm}$ for each run.

---

## Discussion

The present study examined the relative advantages and interchangeability of the traditional MPRAGE and MPRAGE+PMC pulse sequences. Intra-sequence reliabilities demonstrated a clear advantage for the MPRAGE+PMC sequence in a hyperkinetic population, largely due to the compromises in MPRAGE reliability among the higher movers. Inter-sequence reliabilities among low-motion participants demonstrated a high comparability for the assessment of individual differences, suggesting the potential to change sequences mid-study when possible.

In comparison to other studies that directly contrast the MPRAGE and MPRAGE+PMC sequences in a controlled environment, we tested the MPRAGE+PMC sequence in a "real world" scenario, where we did not explicitly ask subjects to move or maintain still during the acquisition of the structural images (Tisdall et al. 2016). All subjects were requested to maintain their head as still as possible throughout the imaging session.

Advantages and Disadvantages

Intra-sequence reliability scores of the two sequences revealed a clear superiority of the newer pulse sequence (MPRAGE-PMC). This was demonstrated across the broad range of morphometric measurements tested. This higher robustness to head motion observed for the MPRAGE-PMC sequence is not only due to the adaptation of the gradients to motion, but the acquisition of TRs with large displacement, which is a novel feature about this sequence (Tisdall et al. 2012) compared to other PMC sequences. Being able to directly estimate head motion though the navigators is also an advantage of the MPRAGE+PMC sequence. These motion measurements can be used post-hoc as a covariate in a statistical analysis or as a proxy on deciding to use or not the structural images.

It is worth noting that not all measurements favored the sequence with PMC. As observed with the quality control indexes, there is a decrease in signal quality in the of the MPRAGE+PMC compared to MPRAGE. The MPRAGE sequence is superior to the MPRAGE+PMC sequence in 5 out of the 7 quality control measurements. Nonetheless, most of the measures in which the MPRAGE sequence is superior depends on the level of noise in the background, which in most part do not affect brain segmentation algorithms (i.e. Freesurfer, Mindboggle, Siena). The CNR, in which MPRAGE+PMC is superior, actually can be considered the most crucial quality control metric (calculates the contrast between the gray matter and the white matter intensities). This contrast is essential for accurately finding the gray matter - white matter boundary, which is imperative for performing segmentation of brain areas/volumes and measuring cortical thickness.

Should researchers switch sequences?

Inter-sequence reliability scores showed excellent mean ICC scores (>0.8) for the majority of the morphometric measures tested. The only exception is cortical thickness, which showed a mean ICC score of 0.512 between MPRAGE1 and MPRAGE+PMC1, showing a higher sensitivity of cortical thickness measurement to motion (Reuter et al. 2015). Consistent with this point, our results show a higher inter-sequence reliability (MPRAGE1 x MPRAGE+PMC1) than intra-sequence reliability of the more traditional sequence (MPRAGE1 x MPRAGE2) in all the morphometric measures. As expected, inter- and intra-sequence reliability is higher for lower motion subjects compared to the higher motion subjects. Analogous results between the two sequences were also obtained for the development curves. This further corroborates with the notion that brain quantitative measures obtained in the different sequences are more equivalent then different.

Taking into account all considerations, we recommend that researchers: 1) use MPRAGE+PMC as their structural T1 weighted pulse imaging sequence for future studies, and 2) consider switching to the MPRAGE+PMC for ongoing studies. While the first recommendation is relatively obvious given our findings that there are higher intra-sequence reliability scores for the MPRAGE+PMC pair (MPRAGE+PMC1 x MPRAGE+PMC1) compared to all other pair of

sequences. In contrast, the second recommendation may be somewhat surprising to some; however, it reflects our findings of high inter-sequence reliability, especially in the MPRAGE1 x MPRAGE-PMC1 pair. The immediate switch to MPRAGE+PMC sequence is likely most important to studies dealing with hyperkinetic populations, where findings are increasingly being questioned due to associations with head motion (Reuter et al. 2015; Alexander-Bloch et al. 2016; Pardoe, Kucharsky Hiess, and Kuzniecky 2016). Neuroimaging researchers with projects studying low head motion participants may very well consider staying with the MPRAGE sequence, possibly finding some advantage given the higher quality control measures.

Beyond the quality control metrics, the only downside that we can identify for adopting the MPRAGE-PMC sequence is the potential increase in acquisition time. However, this increase in acquisition time is mostly due to the repetition of TRs that surpass a motion threshold. If you are studying a population with high motion, on average this is actually an overall reduction in scan time, especially if researchers are considering repeating a full acquisition for high movers. The HBN initiative with children adopted a maximum repeat of 24 TRs. If time is of the essence and the study is with a low moving population, the maximum number of repeated TRs can be reduced to save scanner time.

It is important to note that the MPRAGE+PMC sequence is not entirely immune to head motion and other measures to restrain motion should be used in conjunction with this new sequence. Fortunately, the PMC pulse sequences can be used in conjunction with other strategies for minimizing head movements, such as training the subject in a mock scanner to get acclimated to the environment (de Bie et al. 2010), movie watching to reduce motion (Vanderwal et al. 2015; Greene et al. 2018), and other methods such as using customized head restraints have also been proposed (Power et al. 2019). Additionally, methods that quickly quantify the quality of the structural images have also been proposed (T. White et al. 2018), hence if necessary, a structural scan can quickly be repeated within the same session.

Limitations

This study is limited in the sense that we do not have a direct measurement for motion during the MPRAGE sequence. However, we have attempted to estimate the motion by using the average motion across the functional runs. We have also not performed any rigorous visual inspection (Iscan et al. 2015) or post-processing quality control on the morphometric measurements (Ducharme et al. 2016). We did not want to discard any data due to poor image quality through visual inspection, hence directly comparing the two sequences. As can be seen in Figure 1, though a visual inspection for the high motion participant, we would probably discard the MPRAGE image but not the MPRAGE+PMC image. Another limitation of this study is that the voxel size of the sequences that we are testing have different sizes. However, the objective of this paper is to compare two T1-weighted MRI sequences that are used by a broad number of researchers and by large imaging studies, such as the ABCD study and HCP. Nevertheless, even with different voxel sizes our results showed a high reliability between the two sequences. Finally, we did not perform any statistical corrections for multiple comparisons in any of our tests. The objective of this paper was to uncover if the two sequences are equivalent, not find the differences. Therefore, by using any form of correction for multiple comparisons for our statistical tests would becloud our results.

## Conclusions

Our results indicate that researchers should adopt or switch to the MPRAGE+PMC sequence in their new studies, especially if there are studying populations with high levels of head motion. Morphometric results obtained from the MPRAGE+PMC sequences are comparable to MPRAGE, especially with the low motion images. Hence, there is no loss if a research would choose to switch from MPRAGE to MPRAGE+PMC. Additionally, our data from a developmental study, shows that T1's obtained with PMC have a much higher reliability compared to the traditional MPRAGE sequence. However, quality control metrics have shown higher scores for MPRAGE compared to MPRAGE+PMC, mostly due to increased background noise in the MPRAGE+PMC sequence. Hence, if the population that is being studied has minimal head motion and the researcher would like to maximize data quality (i.e. SNR), the MPRAGE sequence might be preferred.

## Acknowledgments

We would like to thank the participants and parents for participating in the Healthy Brain Network Initiative. We would also like to thank the many individuals who have provided financial support to the CMI Healthy Brain Network to make the creation and sharing of this resource possible and the partial support the NIH grant R01MH091864 to N.T and M.M.

## References

Alexander-Bloch, Aaron, Liv Clasen, Michael Stockman, Lisa Ronan, Francois Lalonde, Jay Giedd, and Armin Raznahan. 2016. "Subtle in-Scanner Motion Biases Automated Measurement of Brain Anatomy from in Vivo MRI." *Human Brain Mapping* 37 (7): 2385–97.

Alexander, Lindsay M., Jasmine Escalera, Lei Ai, Charissa Andreotti, Karina Febre, Alexander Mangone, Natan Vega-Potler, et al. 2017. "An Open Resource for Transdiagnostic Research in Pediatric Mental Health and Learning Disorders." *Scientific Data* 4 (December): 170181.

Atkinson, D., D. L. Hill, P. N. Stoyle, P. E. Summers, and S. F. Keevil. 1997. "Automatic Correction of Motion Artifacts in Magnetic Resonance Images Using an Entropy Focus Criterion." *IEEE Transactions on Medical Imaging* 16 (6): 903–10.

Bie, Henrica M. A. de, Maria Boersma, Mike P. Wattjes, Sofie Adriaanse, R. Jeroen Vermeulen, Kim J. Oostrom, Jaap Huisman, Dick J. Veltman, and Henriette A. Delemarre-Van de Waal. 2010. "Preparing Children with a Mock Scanner Training Protocol Results in High Quality Structural and Functional MRI Scans." *European Journal of Pediatrics* 169 (9): 1079–85.

Bookheimer, Susan Y., David H. Salat, Melissa Terpstra, Beau M. Ances, Deanna M. Barch, Randy L. Buckner, Gregory C. Burgess, et al. 2019. "The Lifespan Human Connectome Project in Aging: An Overview." *NeuroImage* 185 (January): 335–48.

Bookheimer, S. Y. 2000. "Methodological Issues in Pediatric Neuroimaging." *Mental Retardation and Developmental Disabilities Research Reviews* 6 (3): 161–65.

Brant-Zawadzki, M., G. D. Gillan, and W. R. Nitz. 1992. "MP RAGE: A Three-Dimensional, T1-Weighted, Gradient-Echo Sequence--Initial Experience in the Brain." *Radiology* 182 (3): 769–75.

Brown, Robert W., Y. -C. Norman Cheng, E. Mark Haacke, Michael R. Thompson, and Ramesh Venkatesan. 2014. *Magnetic Resonance Imaging: Physical Principles and Sequence Design*. John Wiley & Sons.

Casey, B. J., Tariq Cannonier, May I. Conley, Alexandra O. Cohen, Deanna M. Barch, Mary M. Heitzeg, Mary E. Soules, et al. 2018. “The Adolescent Brain Cognitive Development (ABCD) Study: Imaging Acquisition across 21 Sites.” *Developmental Cognitive Neuroscience*, March. https://doi.org/10.1016/j.dcn.2018.03.001.

Craddock, R. Cameron, Saad Jbabdi, Chao-Gan Yan, Joshua T. Vogelstein, F. Xavier Castellanos, Adriana Di Martino, Clare Kelly, Keith Heberlein, Stan Colcombe, and Michael P. Milham. 2013. “Imaging Human Connectomes at the Macroscale.” *Nature Methods* 10 (6): 524–39.

Ducharme, Simon, Matthew D. Albaugh, Tuong-Vi Nguyen, James J. Hudziak, J. M. Mateos-Pérez, Aurelie Labbe, Alan C. Evans, Sherif Karama, Brain Development Cooperative Group, and Others. 2016. “Trajectories of Cortical Thickness Maturation in Normal Brain Development—the Importance of Quality Control Procedures.” *NeuroImage* 125: 267–79.

Fischl, Bruce. 2012. “FreeSurfer.” *NeuroImage* 62 (2): 774–81.

Giard, Joachim, Patrice Rondao Alface, Jean-Luc Gala, and Benoît Macq. 2011. “Fast Surface-Based Travel Depth Estimation Algorithm for Macromolecule Surface Shape Description.” *IEEE/ACM Transactions on Computational Biology and Bioinformatics / IEEE, ACM* 8 (1): 59–68.

Gilmore, Alysha, Nicholas Buser, and Jamie L. Hanson. 2019. “Variations in Structural MRI Quality Impact Measures of Brain Anatomy: Relations with Age and Other Sociodemographic Variables.” *bioRxiv*. https://doi.org/10.1101/581876.

Glasser, Matthew F., Stephen M. Smith, Daniel S. Marcus, Jesper L. R. Andersson, Edward J. Auerbach, Timothy E. J. Behrens, Timothy S. Coalson, et al. 2016. “The Human Connectome Project’s Neuroimaging Approach.” *Nature Neuroscience* 19 (9): 1175–87.

Greene, Deanna J., Jonathan M. Koller, Jacqueline M. Hampton, Victoria Wesevich, Andrew N. Van, Annie L. Nguyen, Catherine R. Hoyt, et al. 2018. “Behavioral Interventions for Reducing Head Motion during MRI Scans in Children.” *NeuroImage* 171 (May): 234–45.

Harms, Michael P., Leah H. Somerville, Beau M. Ances, Jesper Andersson, Deanna M. Barch, Matteo Bastiani, Susan Y. Bookheimer, et al. 2018. “Extending the Human Connectome Project across Ages: Imaging Protocols for the Lifespan Development and Aging Projects.” *NeuroImage* 183 (December): 972–84.

Howell, Brittany R., Martin A. Styner, Wei Gao, Pew-Thian Yap, Li Wang, Kristine Baluyot, Essa Yacoub, et al. 2019. “The UNC/UMN Baby Connectome Project (BCP): An Overview of the Study Design and Protocol Development.” *NeuroImage* 185 (January): 891–905.

Iscan, Zafer, Tony B. Jin, Alexandria Kendrick, Bryan Szeglin, Hanzhang Lu, Madhukar Trivedi, Maurizio Fava, et al. 2015. “Test-Retest Reliability of Freesurfer Measurements within and between Sites: Effects of Visual Approval Process.” *Human Brain Mapping* 36 (9): 3472–85.

Jack, Clifford R., Jr, Matt A. Bernstein, Nick C. Fox, Paul Thompson, Gene Alexander, Danielle Harvey, Bret Borowski, et al. 2008. “The Alzheimer’s Disease Neuroimaging Initiative (ADNI): MRI Methods.” *Journal of Magnetic Resonance Imaging: JMRI* 27 (4): 685–91.

Jenkinson, Mark, Peter Bannister, Michael Brady, and Stephen Smith. 2002. “Improved Optimization for the Robust and Accurate Linear Registration and Motion Correction of Brain Images.” *NeuroImage* 17 (2): 825–41.

Klein, Arno, Satrajit S. Ghosh, Forrest S. Bao, Joachim Giard, Yrjö Häme, Eliezer Stavsky, Noah Lee, et al. 2017. “Mindboggling Morphometry of Human Brains.” *PLoS Computational Biology* 13 (2): e1005350.

Magnotta, Vincent A., Lee Friedman, and FIRST BIRN. 2006. “Measurement of Signal-to-Noise and Contrast-to-Noise in the fBIRN Multicenter Imaging Study.” *Journal of Digital Imaging* 19 (2): 140–47.

McNEMAR, Q. 1947. “Note on the Sampling Error of the Difference between Correlated

Proportions or Percentages." *Psychometrika* 12 (2): 153–57.
Mortamet, Bénédicte, Matt A. Bernstein, Clifford R. Jack Jr, Jeffrey L. Gunter, Chadwick Ward, Paula J. Britson, Reto Meuli, Jean-Philippe Thiran, Gunnar Krueger, and Alzheimer's Disease Neuroimaging Initiative. 2009. "Automatic Quality Assessment in Structural Brain Magnetic Resonance Imaging." *Magnetic Resonance in Medicine: Official Journal of the Society of Magnetic Resonance in Medicine / Society of Magnetic Resonance in Medicine* 62 (2): 365–72.
Mugler, J. P., 3rd, and J. R. Brookeman. 1990. "Three-Dimensional Magnetization-Prepared Rapid Gradient-Echo Imaging (3D MP RAGE)." *Magnetic Resonance in Medicine: Official Journal of the Society of Magnetic Resonance in Medicine / Society of Magnetic Resonance in Medicine* 15 (1): 152–57.
Nooner, Kate Brody, Stanley J. Colcombe, Russell H. Tobe, Maarten Mennes, Melissa M. Benedict, Alexis L. Moreno, Laura J. Panek, et al. 2012. "The NKI-Rockland Sample: A Model for Accelerating the Pace of Discovery Science in Psychiatry." *Frontiers in Neuroscience* 6 (October): 152.
Pardoe, Heath R., Rebecca Kucharsky Hiess, and Ruben Kuzniecky. 2016. "Motion and Morphometry in Clinical and Nonclinical Populations." *NeuroImage* 135 (July): 177–85.
Power, Jonathan D., Benjamin M. Silver, Melanie R. Silverman, Eliana L. Ajodan, Dienke J. Bos, and Rebecca M. Jones. 2019. "Customized Head Molds Reduce Motion during Resting State fMRI Scans." *NeuroImage* 189 (April): 141–49.
Reuter, Martin, M. Dylan Tisdall, Abid Qureshi, Randy L. Buckner, André J. W. van der Kouwe, and Bruce Fischl. 2015. "Head Motion during MRI Acquisition Reduces Gray Matter Volume and Thickness Estimates." *NeuroImage* 107 (February): 107–15.
Shrout, P. E., and J. L. Fleiss. 1979. "Intraclass Correlations: Uses in Assessing Rater Reliability." *Psychological Bulletin* 86 (2): 420–28.
Smith, Stephen M., Yongyue Zhang, Mark Jenkinson, Jacqueline Chen, P. M. Matthews, Antonio Federico, and Nicola De Stefano. 2002. "Accurate, Robust, and Automated Longitudinal and Cross-Sectional Brain Change Analysis." *NeuroImage* 17 (1): 479–89.
Somerville, Leah H., Susan Y. Bookheimer, Randy L. Buckner, Gregory C. Burgess, Sandra W. Curtiss, Mirella Dapretto, Jennifer Stine Elam, et al. 2018. "The Lifespan Human Connectome Project in Development: A Large-Scale Study of Brain Connectivity Development in 5-21 Year Olds." *NeuroImage* 183 (December): 456–68.
Son, Jake, Lei Ai, Ryan Lim, Ting Xu, Stanley Colcombe, Alexandre Rosa Franco, Jessica Cloud, et al. 2019. "Evaluating fMRI-Based Estimation of Eye Gaze During Naturalistic Viewing." *Cerebral Cortex* , October. https://doi.org/10.1093/cercor/bhz157.
Sudlow, Cathie, John Gallacher, Naomi Allen, Valerie Beral, Paul Burton, John Danesh, Paul Downey, et al. 2015. "UK Biobank: An Open Access Resource for Identifying the Causes of a Wide Range of Complex Diseases of Middle and Old Age." *PLoS Medicine* 12 (3): e1001779.
Tisdall, M. Dylan, Aaron T. Hess, Martin Reuter, Ernesta M. Meintjes, Bruce Fischl, and André J. W. van der Kouwe. 2012. "Volumetric Navigators for Prospective Motion Correction and Selective Reacquisition in Neuroanatomical MRI." *Magnetic Resonance in Medicine: Official Journal of the Society of Magnetic Resonance in Medicine / Society of Magnetic Resonance in Medicine* 68 (2): 389–99.
Tisdall, M. Dylan, Martin Reuter, Abid Qureshi, Randy L. Buckner, Bruce Fischl, and André J. W. van der Kouwe. 2016. "Prospective Motion Correction with Volumetric Navigators (vNavs) Reduces the Bias and Variance in Brain Morphometry Induced by Subject Motion." *NeuroImage* 127 (February): 11–22.
Vanderwal, Tamara, Clare Kelly, Jeffrey Eilbott, Linda C. Mayes, and F. Xavier Castellanos. 2015. "Inscapes: A Movie Paradigm to Improve Compliance in Functional Magnetic

Resonance Imaging." *NeuroImage* 122 (November): 222–32.
Van Essen, David C., Stephen M. Smith, Deanna M. Barch, Timothy E. J. Behrens, Essa Yacoub, Kamil Ugurbil, and WU-Minn HCP Consortium. 2013. "The WU-Minn Human Connectome Project: An Overview." *NeuroImage* 80 (October): 62–79.
White, Nathan, Cooper Roddey, Ajit Shankaranarayanan, Eric Han, Dan Rettmann, Juan Santos, Josh Kuperman, and Anders Dale. 2010. "PROMO: Real-Time Prospective Motion Correction in MRI Using Image-Based Tracking." *Magnetic Resonance in Medicine: Official Journal of the Society of Magnetic Resonance in Medicine / Society of Magnetic Resonance in Medicine* 63 (1): 91–105.
White, Tonya, Philip R. Jansen, Ryan L. Muetzel, Gustavo Sudre, Hanan El Marroun, Henning Tiemeier, Anqi Qiu, Philip Shaw, Andrew M. Michael, and Frank C. Verhulst. 2018. "Automated Quality Assessment of Structural Magnetic Resonance Images in Children: Comparison with Visual Inspection and Surface-Based Reconstruction." *Human Brain Mapping* 39 (3): 1218–31.
Wonderlick, J. S., D. A. Ziegler, P. Hosseini-Varnamkhasti, J. J. Locascio, A. Bakkour, A. van der Kouwe, C. Triantafyllou, S. Corkin, and B. C. Dickerson. 2009. "Reliability of MRI-Derived Cortical and Subcortical Morphometric Measures: Effects of Pulse Sequence, Voxel Geometry, and Parallel Imaging." *NeuroImage* 44 (4): 1324–33.
Yan, Chao-Gan, R. Cameron Craddock, Yong He, and Michael P. Milham. 2013. "Addressing Head Motion Dependencies for Small-World Topologies in Functional Connectomics." *Frontiers in Human Neuroscience* 7 (December): 910.
Zarrar, Shehzad, Giavasis Steven, Li Qingyang, Benhajali Yassine, Yan Chaogan, Yang Zhen, Milham Michael, Bellec Pierre, and Craddock Cameron. 2015. "The Preprocessed Connectomes Project Quality Assessment Protocol - a Resource for Measuring the Quality of MRI Data." *Frontiers in Neuroscience*. https://doi.org/10.3389/conf.fnins.2015.91.00047.

## Supplementary Material

### Supplementary Tables

Supplementary Table 1 (ST1) - Imaging Session Sequence for the Participant that conducted the regular HBN protocol

| Order | Sequence | Time / Run | Cumulative time |
|---|---|---|---|
| 1 | localizer_32ch | 0:00:47 | 0:00:47 |
| 2 | ANAT_T1W-RU(MPRAGE) | 0:07:19 | 0:08:06 |
| 3 | cmrr_fMRI_DistortionMap_AP | 0:00:05 | 0:08:11 |
| 4 | cmrr_fMRI_DistortionMap_PA | 0:00:05 | 0:08:16 |
| 5 | cmrr_REST1 | 0:05:08 | 0:13:24 |
| 6 | cmrr_PEER1 | 0:01:56 | 0:15:20 |
| 7 | cmrr_REST2 | 0:05:08 | 0:20:28 |
| 8 | cmrr_MOVIE1 | 0:10:08 | 0:30:36 |
| 9 | cmrr__dMRI_DistortionMap_AP | 0:00:50 | 0:31:26 |
| 10 | cmrr__dMRI_DistortionMap_PA | 0:00:50 | 0:32:16 |
| 11 | cmrr_DKI_018 | 0:07:55 | 0:40:11 |
| 12 | ABCD_T2w_SPC_vNAV_setter | 0:00:00 | 0:40:11 |
| 13 | ABCD_T2w_SPC_vNav | 0:06:35 | 0:46:46 |
| 14 | ABCD_T1w_MPR_vNAV_setter | 0:00:00 | 0:46:46 |
| 15 | ABCD_T1w_MPR_vNAV(MPRAGE+PMC) | 0:07:12 | 0:53:58 |
| 16 | cmrr_PEER3 | 0:01:56 | 0:55:54 |
| 17 | cmrr_MOVIE2 | 0:03:28 | 0:59:22 |

Supplementary Table 2 (ST2) - Imaging Session Sequence for Participants that conducted the Structural Imaging test-retest protocol.

| Order | Sequence | Time / Run | Cumulative time |
|---|---|---|---|
| 1 | localizer_32ch | 0:00:47 | 0:00:47 |
| 2 | ABCD_T1w_MPR_vNAV_setter | 0:00:00 | 0:00:47 |
| 3 | ABCD_T1w_MPR_vNAV(MPRAGE+PMC_1) | 0:07:12 | 0:07:59 |
| 4 | ANAT_T1W-RU(MPRAGE_1) | 0:07:19 | 0:15:18 |
| 5 | cmrr_fMRI_DistortionMap_AP | 0:00:05 | 0:15:23 |
| 6 | cmrr_fMRI_DistortionMap_PA | 0:00:05 | 0:15:28 |
| 7 | cmrr_REST1 | 0:05:08 | 0:20:36 |
| 8 | cmrr_PEER1 | 0:01:56 | 0:22:32 |
| 9 | cmrr_REST2 | 0:05:08 | 0:27:40 |
| 10 | cmrr_MOVIE1 | 0:10:08 | 0:37:48 |
| 11 | cmrr__dMRI_DistortionMap_AP | 0:00:50 | 0:38:38 |
| 12 | cmrr__dMRI_DistortionMap_PA | 0:00:50 | 0:39:28 |
| 13 | cmrr_DKI_018 | 0:07:55 | 0:47:23 |
| 14 | ABCD_T2w_SPC_vNAV_setter | 0:00:00 | 0:47:23 |
| 15 | ABCD_T2w_SPC_vNav | 0:06:35 | 0:53:58 |
| 16 | ANAT_T1W-RU(MPRAGE_2) | 0:07:19 | 1:01:17 |
| 17 | ABCD_T1w_MPR_vNAV_setter | 0:00:00 | 1:01:17 |
| 18 | ABCD_T1w_MPR_vNAV(MPRAGE+PMC_2) | 0:07:12 | 1:08:29 |
| 19 | cmrr_PEER3 | 0:01:56 | 1:10:25 |
| 20 | cmrr_MOVIE2 | 0:03:28 | 1:13:53 |

Time in between the end of MPRAGE1 and start of MPRAGE2 sequences is 39 minutes
Time in between the end of MPRAGE+PMC1 and start of MPRAGE+PMC2 sequences is 53 minutes

The time between the start of MPRAGE+PMC1 and MPRAGE+PMC2 is at least 1:00:30
Time between the start of MPRAGE1 and MPRAGE2 is at least 0:45:49
Time between the start of MPRAGE+PMC1 and MPRAGE2 is at least 0:53:11
Time between HCP1 and MPRAGE+PMC2 0:53:18

Supplementary Table 3 (ST3) - Correlation scores (Pearson's r) comparing difference in cortical thickness measurements (MPRAGE - MPRAGE+PMC) and mean FD across functional scans. Scores that show significant correlation ($p<0.05$) are color coded, with a positive correlation in red and a negative correlation in blue

| Area | Males | | females | |
|---|---|---|---|---|
| | r-score | p-score | r-score | p-score |
| ctx-lh-caudalanteriorcingulate | -0.090 | 0.225 | -0.307 | 0.001 |
| ctx-lh-caudalmiddlefrontal | -0.231 | 0.002 | -0.504 | 0.000 |
| ctx-lh-cuneus | 0.024 | 0.748 | -0.004 | 0.969 |
| ctx-lh-entorhinal | -0.191 | 0.010 | -0.331 | 0.001 |
| ctx-lh-fusiform | -0.086 | 0.248 | -0.198 | 0.043 |
| ctx-lh-inferiorparietal | -0.195 | 0.008 | -0.352 | 0.000 |
| ctx-lh-inferiortemporal | -0.156 | 0.035 | -0.270 | 0.005 |
| ctx-lh-insula | -0.173 | 0.019 | -0.011 | 0.915 |
| ctx-lh-isthmuscingulate | -0.089 | 0.235 | 0.063 | 0.523 |
| ctx-lh-lateraloccipital | -0.014 | 0.854 | -0.026 | 0.793 |
| ctx-lh-lateralorbitofrontal | -0.145 | 0.051 | -0.132 | 0.180 |
| ctx-lh-lingual | 0.090 | 0.229 | 0.137 | 0.165 |
| ctx-lh-medialorbitofrontal | -0.035 | 0.638 | -0.094 | 0.342 |
| ctx-lh-middletemporal | -0.063 | 0.395 | -0.284 | 0.003 |
| ctx-lh-paracentral | -0.147 | 0.048 | -0.265 | 0.006 |
| ctx-lh-parahippocampal | 0.066 | 0.375 | -0.092 | 0.353 |
| ctx-lh-parsopercularis | -0.293 | 0.000 | -0.185 | 0.059 |
| ctx-lh-parsorbitalis | -0.239 | 0.001 | -0.398 | 0.000 |
| ctx-lh-parstriangularis | -0.156 | 0.036 | -0.220 | 0.024 |
| ctx-lh-pericalcarine | 0.079 | 0.289 | 0.052 | 0.599 |
| ctx-lh-postcentral | -0.097 | 0.195 | -0.032 | 0.746 |
| ctx-lh-posteriorcingulate | -0.044 | 0.555 | -0.220 | 0.024 |
| ctx-lh-precentral | -0.199 | 0.007 | -0.298 | 0.002 |
| ctx-lh-precuneus | -0.183 | 0.013 | -0.190 | 0.052 |
| ctx-lh-rostralanteriorcingulate | 0.094 | 0.206 | 0.117 | 0.235 |
| ctx-lh-rostralmiddlefrontal | -0.205 | 0.006 | -0.357 | 0.000 |
| ctx-lh-superiorfrontal | -0.439 | 0.000 | -0.424 | 0.000 |

| | | | | |
|---|---|---|---|---|
| ctx-lh-superiorparietal | -0.138 | 0.064 | -0.242 | 0.013 |
| ctx-lh-superiortemporal | -0.249 | 0.001 | -0.316 | 0.001 |
| ctx-lh-supramarginal | -0.235 | 0.001 | -0.231 | 0.018 |
| ctx-lh-transversetemporal | -0.112 | 0.133 | -0.238 | 0.014 |
| ctx-rh-caudalanteriorcingulate | 0.051 | 0.493 | -0.113 | 0.251 |
| ctx-rh-caudalmiddlefrontal | -0.212 | 0.004 | -0.399 | 0.000 |
| ctx-rh-cuneus | 0.009 | 0.899 | -0.144 | 0.143 |
| ctx-rh-entorhinal | -0.131 | 0.079 | -0.179 | 0.068 |
| ctx-rh-fusiform | -0.180 | 0.015 | -0.200 | 0.040 |
| ctx-rh-inferiorparietal | -0.116 | 0.119 | -0.301 | 0.002 |
| ctx-rh-inferiortemporal | -0.205 | 0.006 | -0.363 | 0.000 |
| ctx-rh-insula | -0.048 | 0.523 | 0.083 | 0.399 |
| ctx-rh-isthmuscingulate | 0.106 | 0.156 | 0.091 | 0.356 |
| ctx-rh-lateraloccipital | 0.038 | 0.607 | -0.070 | 0.479 |
| ctx-rh-lateralorbitofrontal | -0.124 | 0.095 | -0.222 | 0.023 |
| ctx-rh-lingual | 0.202 | 0.006 | 0.021 | 0.828 |
| ctx-rh-medialorbitofrontal | 0.140 | 0.059 | -0.113 | 0.249 |
| ctx-rh-middletemporal | -0.123 | 0.097 | -0.275 | 0.005 |
| ctx-rh-paracentral | -0.214 | 0.004 | -0.129 | 0.190 |
| ctx-rh-parahippocampal | 0.100 | 0.178 | -0.047 | 0.632 |
| ctx-rh-parsopercularis | -0.075 | 0.317 | -0.303 | 0.002 |
| ctx-rh-parsorbitalis | -0.236 | 0.001 | -0.142 | 0.149 |
| ctx-rh-parstriangularis | -0.030 | 0.686 | -0.343 | 0.000 |
| ctx-rh-pericalcarine | 0.159 | 0.032 | 0.088 | 0.372 |
| ctx-rh-postcentral | 0.078 | 0.293 | 0.046 | 0.644 |
| ctx-rh-posteriorcingulate | 0.080 | 0.280 | -0.025 | 0.798 |
| ctx-rh-precentral | -0.188 | 0.011 | -0.315 | 0.001 |
| ctx-rh-precuneus | -0.057 | 0.448 | 0.150 | 0.125 |
| ctx-rh-rostralanteriorcingulate | 0.016 | 0.831 | -0.034 | 0.728 |
| ctx-rh-rostralmiddlefrontal | -0.125 | 0.093 | -0.275 | 0.005 |
| ctx-rh-superiorfrontal | -0.313 | 0.000 | -0.476 | 0.000 |
| ctx-rh-superiorparietal | -0.147 | 0.048 | -0.159 | 0.105 |

| | | | | |
|---|---|---|---|---|
| ctx-rh-superiortemporal | -0.136 | 0.067 | -0.206 | 0.035 |
| ctx-rh-supramarginal | -0.133 | 0.074 | -0.208 | 0.033 |
| ctx-rh-transversetemporal | -0.206 | 0.005 | 0.030 | 0.763 |

Supplementary Table 4 (ST4) - Paired t-test results comparing cortical thickness measurements from MPRAGE and MPRAGE+PMC images. Scores that show significant differences ($p<0.05$) are color coded, with MPRAGE>MPRAGE+PMC in red and MPRAGE+PMC>MPRAGE in blue.

| Area | Males | | Females | |
|---|---|---|---|---|
| | t-score | p-score | t-score | p-score |
| ctx-lh-caudalanteriorcingulate | 5.328 | 0.000 | 5.973 | 0.000 |
| ctx-lh-caudalmiddlefrontal | -0.214 | 0.831 | 0.853 | 0.395 |
| ctx-lh-cuneus | -2.760 | 0.006 | -3.132 | 0.002 |
| ctx-lh-entorhinal | -4.399 | 0.000 | -2.892 | 0.005 |
| ctx-lh-fusiform | 5.151 | 0.000 | 3.708 | 0.000 |
| ctx-lh-inferiorparietal | 2.804 | 0.006 | 2.187 | 0.031 |
| ctx-lh-inferiortemporal | 1.712 | 0.089 | 1.334 | 0.185 |
| ctx-lh-insula | 1.776 | 0.077 | 2.094 | 0.039 |
| ctx-lh-isthmuscingulate | 10.844 | 0.000 | 7.557 | 0.000 |
| ctx-lh-lateraloccipital | 2.377 | 0.019 | -0.043 | 0.966 |
| ctx-lh-lateralorbitofrontal | -2.453 | 0.015 | -1.857 | 0.066 |
| ctx-lh-lingual | -5.114 | 0.000 | -4.036 | 0.000 |
| ctx-lh-medialorbitofrontal | 4.704 | 0.000 | 0.801 | 0.425 |
| ctx-lh-middletemporal | 2.795 | 0.006 | 1.067 | 0.289 |
| ctx-lh-paracentral | 1.881 | 0.062 | 3.761 | 0.000 |
| ctx-lh-parahippocampal | 3.959 | 0.000 | 2.933 | 0.004 |
| ctx-lh-parsopercularis | 1.086 | 0.279 | 3.204 | 0.002 |
| ctx-lh-parsorbitalis | 1.121 | 0.264 | -0.077 | 0.939 |
| ctx-lh-parstriangularis | 2.299 | 0.023 | 2.889 | 0.005 |
| ctx-lh-pericalcarine | -6.639 | 0.000 | -5.601 | 0.000 |
| ctx-lh-postcentral | -2.379 | 0.018 | -1.910 | 0.059 |
| ctx-lh-posteriorcingulate | 7.968 | 0.000 | 5.660 | 0.000 |
| ctx-lh-precentral | -1.531 | 0.127 | 0.438 | 0.663 |
| ctx-lh-precuneus | 3.221 | 0.002 | 4.850 | 0.000 |
| ctx-lh-rostralanteriorcingulate | 5.364 | 0.000 | 3.508 | 0.001 |
| ctx-lh-rostralmiddlefrontal | 1.067 | 0.287 | 0.351 | 0.727 |
| ctx-lh-superiorfrontal | 2.231 | 0.027 | 3.538 | 0.001 |

| | | | | |
|---|---|---|---|---|
| ctx-lh-superiorparietal | -0.214 | 0.831 | 0.597 | 0.552 |
| ctx-lh-superiortemporal | 1.584 | 0.115 | 1.826 | 0.071 |
| ctx-lh-supramarginal | 0.352 | 0.725 | 2.838 | 0.005 |
| ctx-lh-transversetemporal | -1.900 | 0.059 | -0.595 | 0.553 |
| ctx-rh-caudalanteriorcingulate | 8.937 | 0.000 | 3.179 | 0.002 |
| ctx-rh-caudalmiddlefrontal | -1.528 | 0.128 | 1.806 | 0.074 |
| ctx-rh-cuneus | -5.525 | 0.000 | -3.309 | 0.001 |
| ctx-rh-entorhinal | -4.544 | 0.000 | -2.637 | 0.010 |
| ctx-rh-fusiform | -0.200 | 0.842 | -0.420 | 0.675 |
| ctx-rh-inferiorparietal | 0.617 | 0.538 | 0.594 | 0.554 |
| ctx-rh-inferiortemporal | -1.619 | 0.107 | -2.151 | 0.034 |
| ctx-rh-insula | 2.542 | 0.012 | 3.610 | 0.000 |
| ctx-rh-isthmuscingulate | 11.244 | 0.000 | 6.875 | 0.000 |
| ctx-rh-lateraloccipital | 0.689 | 0.492 | 0.162 | 0.872 |
| ctx-rh-lateralorbitofrontal | 2.267 | 0.025 | 2.155 | 0.033 |
| ctx-rh-lingual | -5.142 | 0.000 | -6.648 | 0.000 |
| ctx-rh-medialorbitofrontal | 10.090 | 0.000 | 6.102 | 0.000 |
| ctx-rh-middletemporal | 2.641 | 0.009 | 1.791 | 0.076 |
| ctx-rh-paracentral | 3.021 | 0.003 | 4.251 | 0.000 |
| ctx-rh-parahippocampal | 1.928 | 0.055 | 1.237 | 0.219 |
| ctx-rh-parsopercularis | 3.951 | 0.000 | 3.690 | 0.000 |
| ctx-rh-parsorbitalis | 1.911 | 0.058 | 2.439 | 0.016 |
| ctx-rh-parstriangularis | 3.512 | 0.001 | 2.306 | 0.023 |
| ctx-rh-pericalcarine | -8.103 | 0.000 | -5.649 | 0.000 |
| ctx-rh-postcentral | -2.150 | 0.033 | -1.846 | 0.068 |
| ctx-rh-posteriorcingulate | 10.669 | 0.000 | 8.325 | 0.000 |
| ctx-rh-precentral | -1.148 | 0.253 | -0.214 | 0.831 |
| ctx-rh-precuneus | 5.422 | 0.000 | 5.526 | 0.000 |
| ctx-rh-rostralanteriorcingulate | 8.657 | 0.000 | 6.225 | 0.000 |
| ctx-rh-rostralmiddlefrontal | 0.840 | 0.402 | 0.484 | 0.630 |
| ctx-rh-superiorfrontal | 3.426 | 0.001 | 3.828 | 0.000 |
| ctx-rh-superiorparietal | -1.216 | 0.226 | -0.993 | 0.323 |

| | | | | |
|---|---|---|---|---|
| ctx-rh-superiortemporal | 3.902 | 0.000 | 2.997 | 0.003 |
| ctx-rh-supramarginal | 1.143 | 0.254 | 0.931 | 0.354 |
| ctx-rh-transversetemporal | -0.364 | 0.716 | 3.265 | 0.001 |

## Supplementary Figures

Supplementary Figure 1 (SF1) - Location of circles for calculating Anterior-to-Superior Ratio (ASR).

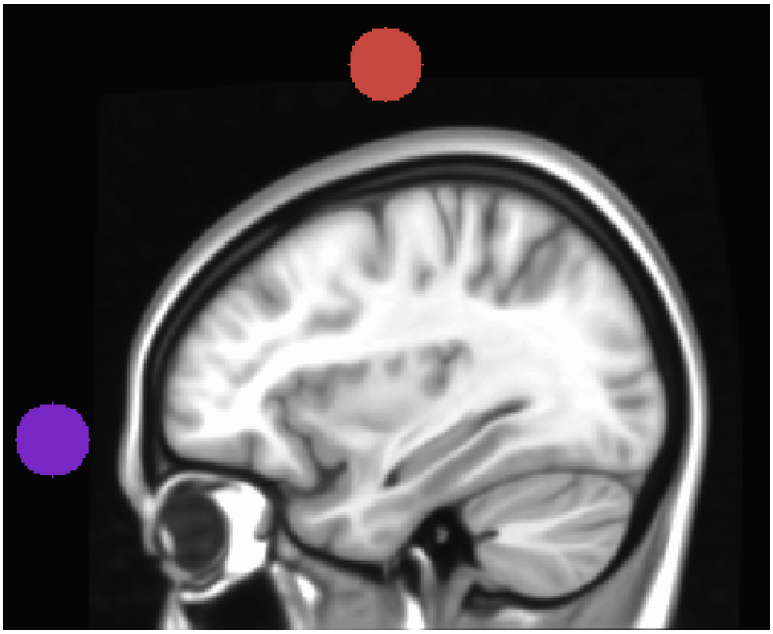

Supplementary Figure 2 (SF2) - Images with high motion for MPRAGE+PMC runs

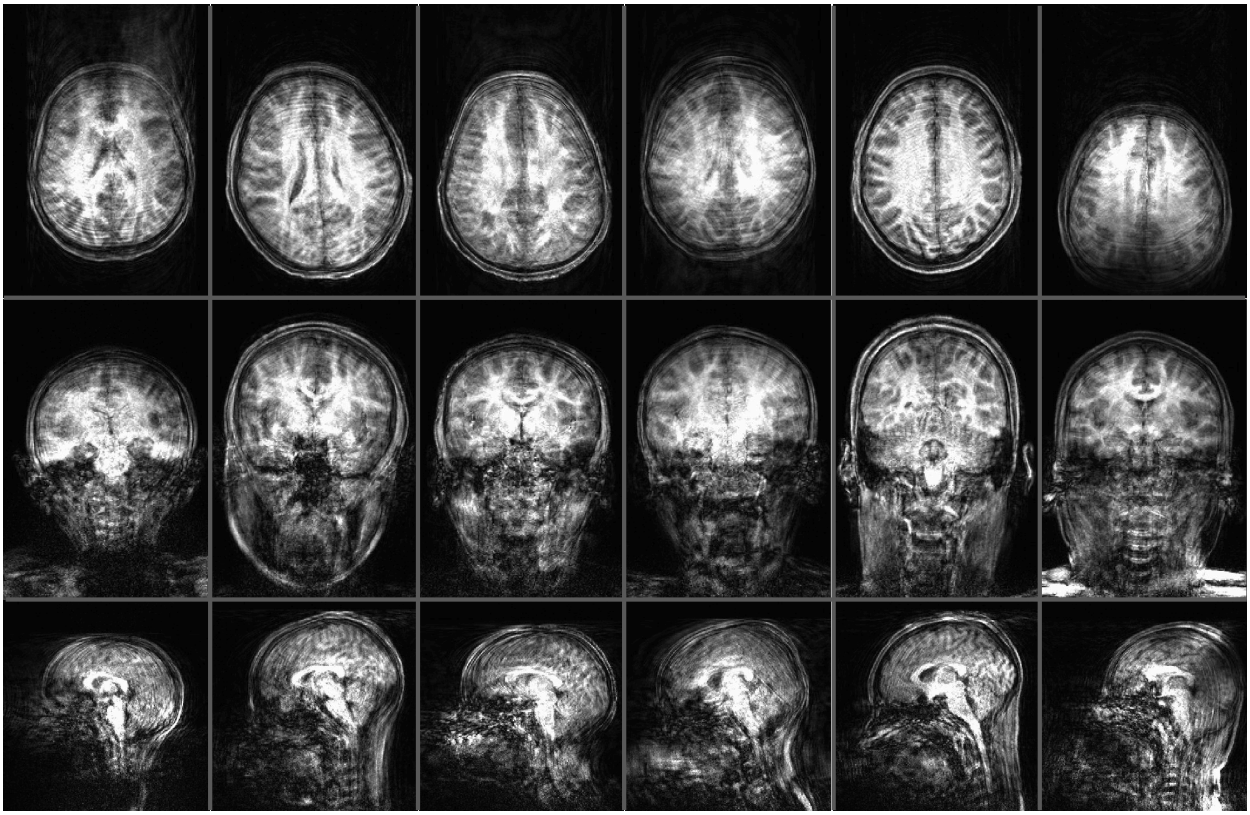

Supplementary Figure 3 (SF3) - Cortical thickness difference (MPRAGE - MPRAGE+PMC) X Framewise Displacement ($FD_{pm}$) for males. Subplot titles are color coded in red if there was a significant ($p<0.05$) correlation.

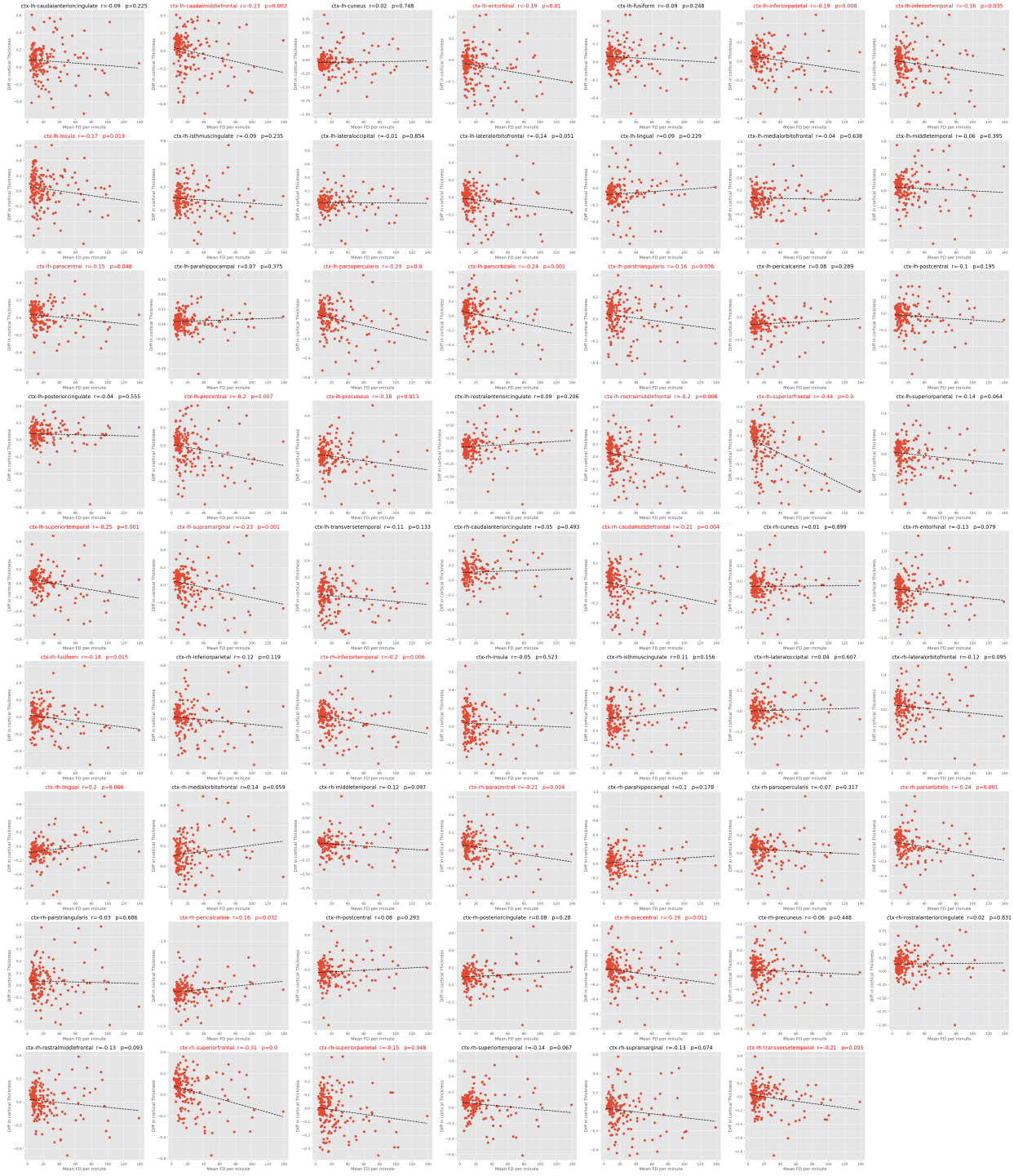

Supplementary Figure 4 (SF4) - Cortical thickness difference (MPRAGE - MPRAGE+PMC) X Framewise Displacement ($FD_{pm}$) for females. Subplot titles are color coded in red if there was a significant ($p<0.05$) correlation.

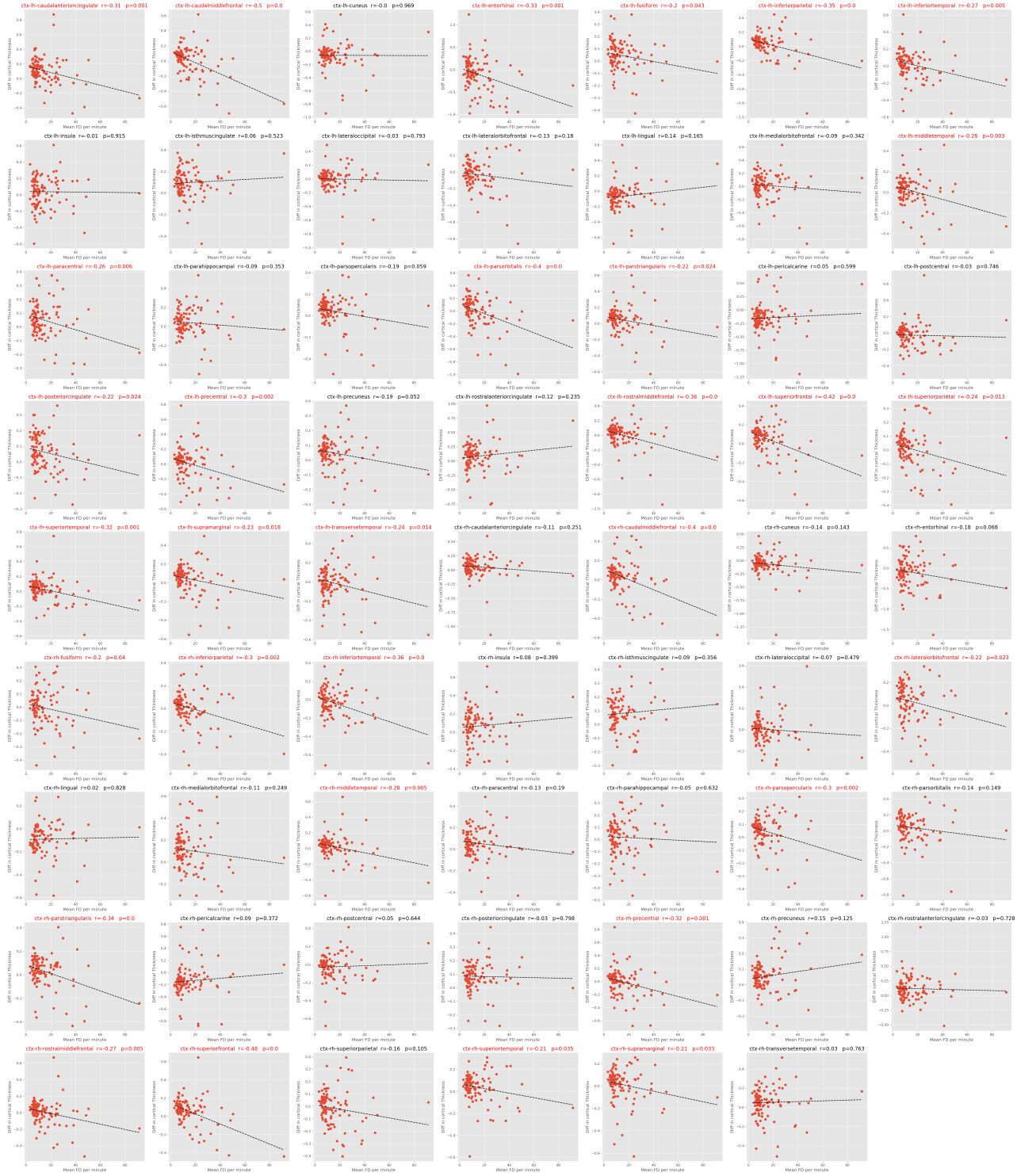

Supplementary Figure 5 (SF5) - Paired t-test results comparing cortical thickness measurements from MPRAGE and MPRAGE+PMC images. Regions of the brain with significant difference ($p<0.05$) are color-coded based on t-scores from the paired t-test, where warm colors represent MPRAGE > MPRAGE+PMC and cold colors represent MPRAGE+PMC > MPRAGE.

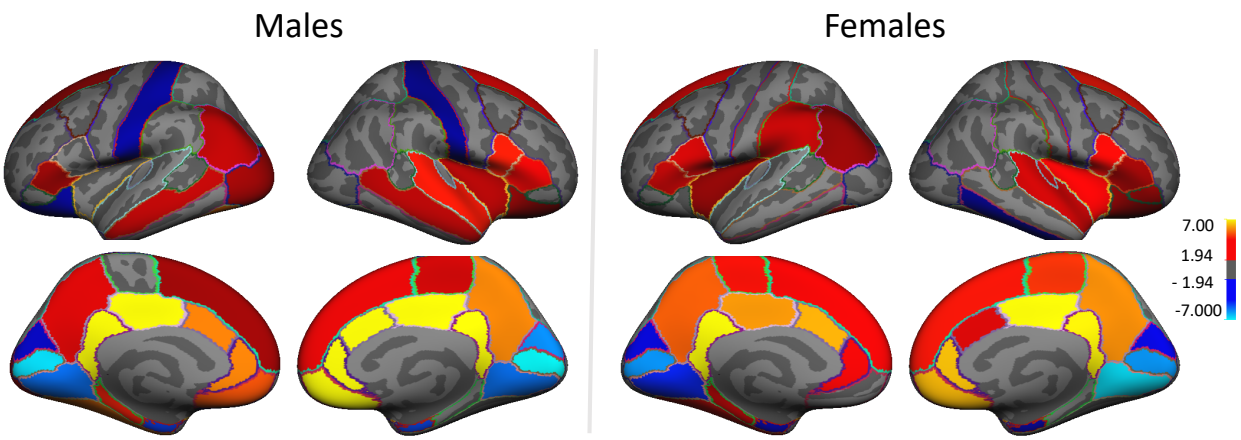

Supplementary Figure 6 (SF6) - Cortical Thickness Development curves for Males. Back lines represent the MPRAGE sequence, while red represents that MPRAGE+PMC sequence.

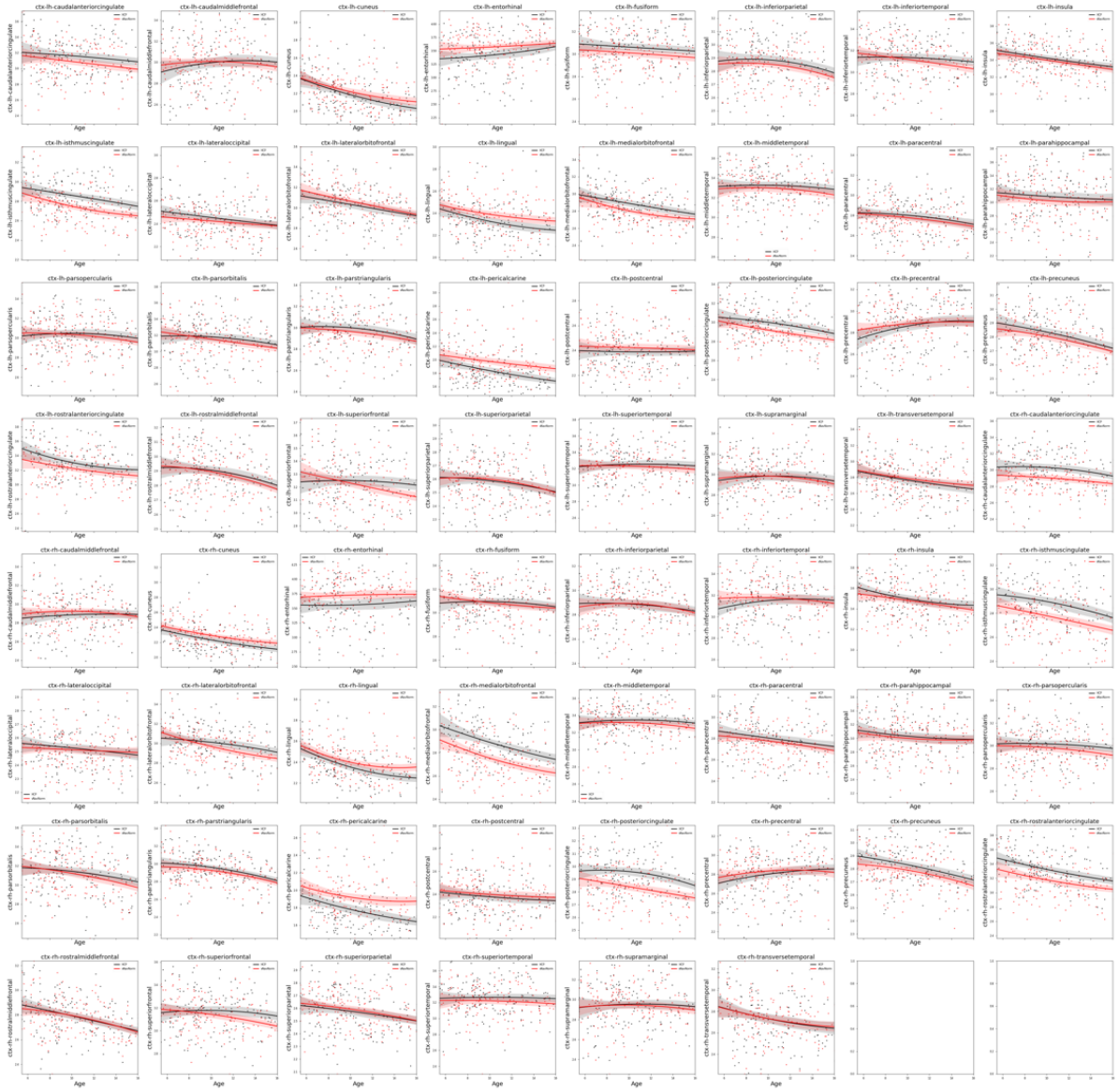

Supplementary Figure 7 (SF7) - Cortical Thickness Development curves for Females. Back lines represent the MPRAGE sequence, while red represents that MPRAGE+PMC sequence.

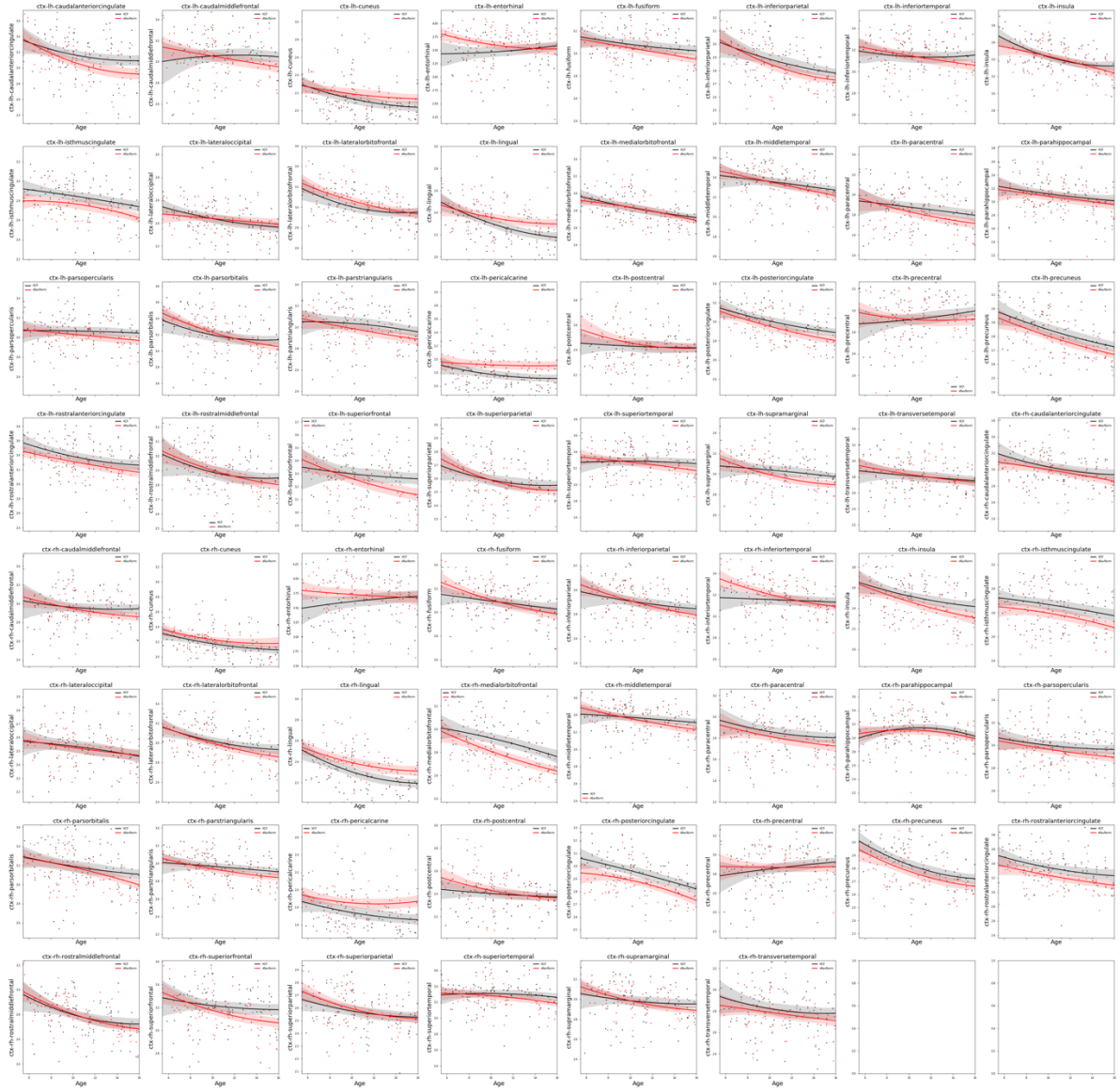

Supplementary Figure 8 (SF8) - Quality Control Metrics for the test-retest group.